Virology 449 (2014) 270–286

Contents lists available at ScienceDirect

Virology

journal homepage: www.elsevier.com/locate/yviro

Reactive oxygen species activate NFκB (p65) and p53 and induce apoptosis in RVFV infected liver cells

Aarthi Narayanan [a,1], Moushimi Amaya [a,1], Kelsey Voss [a], Myung Chung [a], Ashwini Benedict [a], Gavin Sampey [a], Kylene Kehn-Hall [a], Alessandra Luchini [b], Lance Liotta [b], Charles Bailey [a], Ajit Kumar [c], Sina Bavari [d], Ramin M. Hakami [a], Fatah Kashanchi [a,*]

[a] National Center for Biodefense and Infectious Diseases, and the School of Systems Biology, George Mason University, Manassas, VA, USA
[b] Center for Applied Proteomics and Personalized Medicine, George Mason University, Manassas, VA, USA
[c] George Washington Medical School, Washington DC, USA
[d] United States Army Medical Research Institute for Infectious Diseases, Fredrick, MD, USA

ARTICLE INFO

Article history:
Received 8 July 2013
Returned to author for revisions
2 August 2013
Accepted 17 November 2013
Available online 15 December 2013

Keywords:
Reactive oxygen species
p65
p53
Apoptosis
Liver cells
Rift Valley fever virus

ABSTRACT

Rift Valley fever virus (RVFV) infection is often associated with pronounced liver damage. Previously, our studies revealed altered host phospho-signaling responses (NFκB, MAPK and DNA damage responses) in RVFV infected epithelial cells that correlated with a cellular stress response. Here, we report that RVFV infection of liver cells leads to an increase in reactive oxygen species (ROS). Our data suggests the presence of the viral protein NSs in the mitochondria of infected cells, hence contributing to early increase in ROS. Increased ROS levels correlated with activation of NFκB (p65) and p53 responses, which in conjunction with infection, was also reflected as macromolecular rearrangements observed using size fractionation of protein lysates. Additionally, we documented an increase in cytokine expression and pro-apoptotic gene expression with infection, which was reversed with antioxidant treatment. Collectively, we identified ROS and oxidative stress as critical contributors to apoptosis of liver cells during RVFV infection.

Introduction

Rift Valley fever virus (RVFV) is an arbovirus belonging to the genus *Phlebovirus*, family *Bunyaviridae* (Ikegami and Makino, 2011; Weaver and Reisen, 2010; Bouloy and Weber, 2010; Ikegami, 2012). The viral genome is a single stranded RNA, which exists as three segments namely, large (L), medium (M) and small (S) (Terasaki et al., 2011; Gauliard et al., 2006; Ikegami et al., 2005a, 2005b). The L segment codes for the viral RNA dependent RNA polymerase. The M segment codes for the two structural proteins Gn and Gc and two nonstructural proteins, 78 kDa protein and NSm. The S segment codes for the N protein and the nonstructural protein NSs. NSs plays an essential role in the viral life cycle by down regulating the host innate immune response early in infection (Kalveram et al., 2011, 2013; Benferhat et al., 2012; Mansuroglu et al., 2010; Ikegami et al., 2009a, 2009b; Habjan et al., 2009; Le May et al., 2008). NSm protein has been demonstrated to have an anti-apoptotic function in infected cells (Won et al., 2007).

RVFV is mainly transmitted by mosquitoes, although other arthropods including flies have also been demonstrated to be adequate hosts (Amraoui et al., 2012; Turell et al., 2008, 2010a, 2010b; Seufi and Galal, 2010). Viral infection of humans results in Rift Valley Fever (RVF) with flu-like symptoms (Ikegami and Makino, 2011). RVFV infections are often accompanied by liver damage. In a small percentage of cases, RVF can result in hemorrhage and neuronal phenotypes. Viral infection of livestock results in abortion rates that can reach 100% and high fatality among newborns (Ikegami and Makino, 2011; Bouloy and Weber, 2010). RVFV is classified as a category A select agent, an emerging infectious agent and an agricultural pathogen. The currently available vaccine candidates include mutant viruses (deleted for NSs, NSm segments), vaccines based on structural proteins, reconstructed virions, viral replicon particles or serially passaged attenuated virus (Bird et al., 2011; Kortekaas et al., 2012; Dodd et al., 2012; Kalveram et al., 2011; Jansen van Vuren et al., 2011; Morrill and Peters, 2011; Pichlmair et al., 2010; de Boer et al., 2010; Mandell et al., 2010; Ikegami and Makino, 2009). These candidates however, have not yet been approved for human use.

* Correspondence to: National Center for Biodefense and Infectious Diseases, George Mason University, Discovery Hall, Room 182, 10900 University Blvd, MS 1H8, Manassas, VA, USA. Tel. +1 703 993 9160, fax: +1 703 993 7022.
E-mail address: fkashanc@gmu.edu (F. Kashanchi).
[1] Contributed equally.

0042-6822/$ - see front matter © 2013 Elsevier Inc. All rights reserved.
http://dx.doi.org/10.1016/j.virol.2013.11.023

Interactions between the virus and its host have been subject to intense investigation by multiple laboratories as this can provide critical information for the development of novel diagnostic and therapeutic avenues. Our previous approaches to understand host–pathogen interactions of RVFV and its human host using Reverse Phase Protein MicroArray (RPMA) have yielded significant information about host responses in infected cells (Popova et al., 2010). We have shown that RVFV infection of human cells induced multiple shifts in the anti- and pro-apoptotic pathways at early and late stages of infection. RVFV infection resulted in activation of stress responses and DNA damage responses (DDR) (Narayanan et al., 2011; Baer et al., 2012). Additionally, RVFV infection induced activation of critical transcription factors including NFκB (p65) and p53 (Narayanan et al., 2012; Austin et al., 2012). Our laboratory and those of our colleagues have demonstrated that inhibition of host responses during RVFV infection is a viable method to inhibit viral multiplication and afford protection to the host (Popova et al., 2010; Baer et al., 2012; Narayanan et al., 2012; Moser et al., 2012; Filone et al., 2010).

Studies with animal model systems have demonstrated that RVFV infection induces apoptotic responses in the liver of infected animals (Smith et al., 2010, 2012; Reed et al., 2012; Ding et al., 2005). Notably, strong inflammatory responses including cytokine secretion have been indicated to be involved in the apoptotic outcome in infected livers. Oxidative stress following infection is a key component that influences disease outcome in the host in the case of multiple viral infections including Hepatitis B virus (HBV), Hepatitis C virus (HCV), Human Immunodeficiency Virus (HIV), and Crimean Congo Hemorrhagic Fever virus (CCHF) (Duygu et al., 2012; Tawadrous et al., 2012; Lin et al., 2011; Rodrigues et al., 2012). Many viral proteins have been demonstrated to actively modulate the host oxidative stress responses to facilitate replication. For example, the viral core protein of HCV was shown to increase oxidative stress in HepG2 cells by interfering with the heme oxygenase mediated host response (Abdalla et al., 2012). HCV proteins including E1 and E2 were demonstrated to activate the antioxidant defense Nrf2/ARE pathway via several independent mechanisms (Ivanov et al., 2011). HCV nonstructural proteins contribute to pathogenesis by influencing mitochondrial redox potential ending in mitochondrial injury and apoptosis in liver cells (Abdalla et al., 2005; Gong et al., 2001). Use of antioxidants has had beneficial effects in HCV patients by attenuating multiple oxidative stress induced responses (Farias et al., 2012).

Reactive oxygen species (ROS) is an important host component that contributes to the innate immune response against multiple pathogens. ROS production may directly influence pathogen killing as seen in the case of infected macrophages (Jaeschke, 2011). ROS are also secondary signaling messengers that activate many host phospho-signaling responses including the nuclear factor kappa beta (NFkB), activating protein-1 (AP-1), mitogen-activating protein kinase (MAPK), phosphotidyl inositol-3 kinase (PI3K) and DNA damage response (DDR) pathways (Waris et al., 2001; Gwinn and Vallyathan 2006; Yang et al., 2010; Imai et al., 2008). Activation of transcription factors such as p65 and p53 due to increased intracellular ROS contributes to the inflammatory responses such as cytokine secretion.

In this manuscript, we have investigated the early onset of oxidative stress that leads to apoptotic responses in RVFV-infected liver cells. Our working hypothesis was that RVFV infection-induced oxidative stress activated both p65 and p53, which in turn modulated cytokine secretion and apoptotic gene expression profiles leading to cell death. Therefore, amelioration of oxidative stress in infected cells using antioxidants would decrease inflammatory cytokine expression, and apoptotic gene expression. Our data indicate that p65 activation occurred early in the temporal sequence of events after RVFV infection while p53 activation occurred at later time points. Antioxidants down regulated expression of inflammatory cytokines and apoptotic gene expression in liver cells. Therefore, antioxidants warrant further examination as a potential therapeutic strategy to achieve hepatoprotection in RVFV infections.

Results

HepG2 cells display increased reactive oxygen species following RVFV infection

We had demonstrated in our earlier studies that RVFV infection of epithelial cells resulted in increased expression of superoxide dismutase, an enzyme that is involved in oxidative stress response (Narayanan et al., 2011). The liver is one of the most prominently affected organs during RVFV infection. Oxidative stress has been demonstrated to play a critical role in liver pathologies both in the case of cancer and in virus infections such as HCV (Tawadrous et al., 2012). In many of these pathological responses in the liver, the outcome was associated with the host inflammatory responses including production of cytokines and resultant apoptosis (Duygu et al., 2012; Tawadrous et al., 2012; Lin et al., 2011). Therefore, we attempted to analyze oxidative stress and associated cytokine responses in RVFV infected liver cells. We first examined the generation of ROS in RVFV infected HepG2 cells following infection. HepG2 cells were infected with the MP-12 strain of RVFV, fixed and stained using MitoSox stain at 3 h post infection.

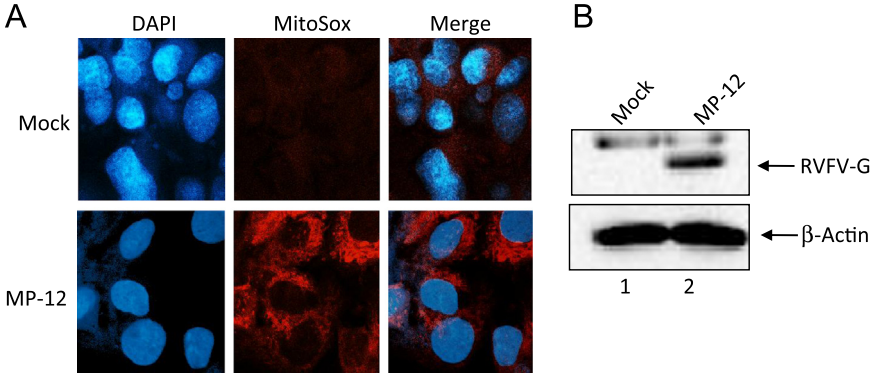

Fig. 1. Increased ROS in RVFV infected HepG2 cells. (A) HepG2 cells were infected with the MP-12 strain of RVFV (MOI: 3) and stained after 3 h using MitoSox stain and DAPI. The stained cells were visualized by confocal microscopy. (B) HepG2 cells infected with MP-12 (MOI: 3) were lysed at 24 h post infection and total protein lysate obtained. Lysates from uninfected cells were obtained as controls and both lysates were resolved by SDS-PAGE and western blots, carried out using anti-RVFV and anti-β-actin antibodies.

MitoSox is a fluorescent probe that is employed to measure superoxide in cells and therefore can be utilized to analyze the general superoxide content of the cell (Narayanan et al., 2011). Upon MitoSox staining of HepG2 cells that were either mock infected or infected with MP-12, we observed an increase in superoxide levels in the infected cells (Fig. 1A). Quantification of the fluorescence revealed an approximate 6-fold increase in superoxide levels in virus-infected cells over the mock-infected controls. Western blots were performed to detect expression of viral proteins (glycoprotein) in infected cells to validate infection and viral multiplication (Fig. 1B).

We then asked if the viral nonstructural proteins NSs and NSm played a role in the generation of superoxide species at early and late stages of infection. We infected HepG2 cells with either the wild type virus (MP-12) or deletion mutants (MP-12ΔNSs; MP-12ΔNSm) and MitoSox-stained fixed cells at early (6 h post infection) and late (24 h post infection) time points. These mutant viruses do not display any significant differences in replication

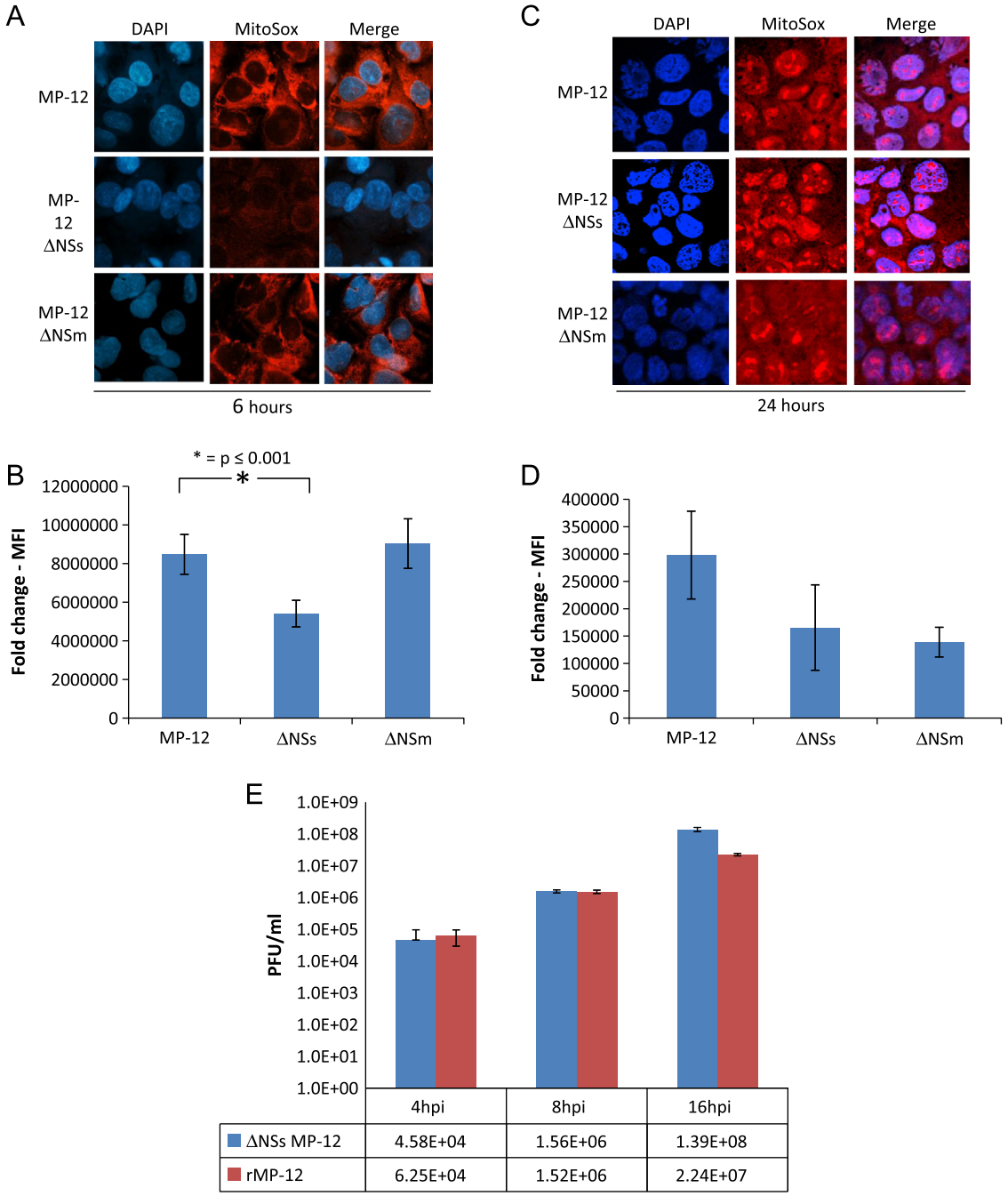

	4hpi	8hpi	16hpi
ΔNSs MP-12	4.58E+04	1.56E+06	1.39E+08
rMP-12	6.25E+04	1.52E+06	2.24E+07

Fig. 2. NSs protein influences early stages of ROS accumulation in infected HepG2 cells. (A) and (C) HepG2 cells were infected with MP-12, MP-12ΔNSs and MP-12ΔNSm virus strains (MOI: 3) and stained after 6 h and 24 h respectively using MitoSox stain and DAPI. Images of stained cells were obtained by confocal microscopy. (B) and (D) Fold changes in mean fluorescence intensities (MFIs) were obtained by comparing fluorescence intensities of 10 randomly chosen fields of MP-12, MP-12ΔNSs and MP-12ΔNSm infected cells ($n > 75$ cells). (E) HepG2 cells were infected with either recombinant MP-12 (rMP-12) or MP-12ΔNSs (MOI: 3) and supernatants collected at 4, 8 and 16 h post infection. Supernatants were used to perform plaque assays as described in the materials and methods section. Results are represented graphically as replication kinetics of rMP-12 and MP-12ΔNSs. The average number of PFU/mL is tabulated below and shows the average of three biological replicates plated in technical duplicates. Error bars indicate the standard deviation for all 6 data points across the triplicate sample groups.

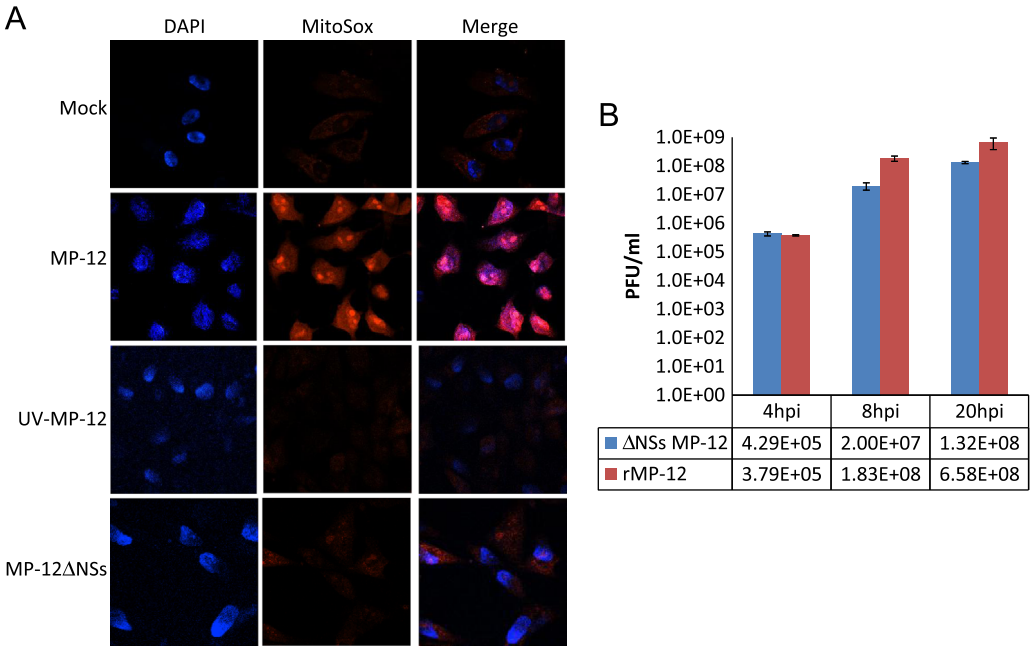

Fig. 3. Increased ROS in MP-12 infected Vero cells. (A) Vero cells were mock infected or infected with MP-12, UV-MP-12 and MP-12ΔNSs (MOI: 3) and stained after 3 h using MitoSox stain and DAPI. Images of stained cells were obtained by confocal microscopy. (B) Vero cells were infected with either recombinant MP-12 or MP-12ΔNSs (MOI: 3) and supernatants collected at 4, 8 and 20 h post infection. Supernatants were used to perform plaque assays as described in the materials and methods section. The graph represents the replication kinetics of rMP-12 and MP-12ΔNSs. The average number of PFU/mL is tabulated below and shows the average of three biological replicates plated in technical duplicates. Error bars indicate the standard deviation for all 6 data points across the triplicate sample groups.

kinetics compared to the parental MP-12 strain (Won et al., 2007; Narayanan et al., 2012). The experiment revealed that at 6 h post infection, the NSs deletion virus resulted in lower levels of superoxide species in the infected cells when compared to the wild type virus or the NSm mutant (Fig. 2A) and quantification of Mean Fluorescence Intensity for fields of cells (MFI) revealed a statistically significant decrease (Fig. 2B). To calculate fold changes in MFIs, we compared fluorescent intensities of 10 randomly chosen fields of MP-12, MP-12ΔNSs and MP-12ΔNSm infected cells ($n > 75$ cells).

Interestingly, when we analyzed cells at later time points (24 h post infection), we did not observe statistically significant differences in intracellular superoxide levels of cells infected with either the wild type or the mutant viruses (Fig. 2C and D). We observed that at early time points after infection, superoxide species were largely restricted to the cytoplasm while at later time points, we detected superoxide species inside the nucleus as well (Fig. 2C). Nuclear accumulation of superoxide species may be indicative of a wide spread disruption of homeostasis and the cellular oxidative response machinery at later time points in RVFV-infected liver cells. Viral infections of hepatocytes such as HCV have demonstrated to increase perinuclear ROS levels, primarily involving deregulated host antioxidant machinery including NADPH oxidases (Beckman and Koppenol, 1996; Ushio-Fukai, 2009). Next, we asked whether differences in early MitoSox staining, and hence levels of superoxide species, between MP-12 and MP-12ΔNSs could be a result of differences in replication kinetics between the two viral strains. We performed plaque assays to quantify replication kinetics of both viruses in HepG2 cells and the results suggested that the two viral strains did not differ appreciably in their replication (Fig. 2E).

We then asked if the observed phenotype of early NSs-dependent accumulation of superoxide in infected cells could be influenced by interferon. Interferon regulation is an important aspect of NSs function in RVFV infection. To that end, we used Vero cells, which are known to be deficient in interferon production. We infected Vero cells with MP-12, UV-inactivated MP-12, and MP-12ΔNSs viruses. Mock-infected cells were maintained as controls. The infected cells were stained with MitoSox at an early time point and visualized for accumulation of superoxide species. As shown in Fig. 3A, the accumulation of superoxide was maximum in MP-12 infected cells similar to what we had observed in HepG2 cells. Evaluation of replication kinetics of MP-12 and MP-12ΔNSs in the Vero cell line did not reveal any major difference between the two strains (Fig. 3B).

Cumulatively, our studies reveal that RVFV infection of liver cells results in a significant increase in intracellular ROS levels after infection. Furthermore, results suggest that while the viral protein NSs may play a role in the onset of oxidative stress at early time points after infection, the onset of oxidative stress in infected cells at later time points was independent of NSs.

The viral protein NSs is associated with the mitochondria in RVFV-infected liver cells

Our observation that infection by the NSs mutant virus resulted in a statistically significant decrease in ROS production in the infected cells at early time points prompted the question of whether NSs itself was associated with the mitochondria of infected cells. The mitochondria are the primary organelles that contribute to intracellular ROS levels as a part of the normal cellular respiratory process. Deregulation of the mitochondrial respiratory chain is observed during multiple disease states that leads to ROS mediated pathology. Although nuclear functions of NSs have been well documented, approximately 50% of the NSs protein expressed in an infected cell is cytoplasmic at early hours (Kehn Hall, personal communication). To determine if NSs displayed an association with the mitochondria in infected cells, we infected HepG2 cells with a Flag-tagged NSs (Flag-NSs-MP-12) containing virus. The infected cells were lysed and NSs immunoprecipitated with an antibody against the Flag tag. The immunoprecipitated material was directly processed for LC-MS/MS analysis where the proteins were eluted from protein A/G beads by 8M Urea and trypsinized. LC-MS/MS analysis of the trypsinized

A

Reference	P (pro)	Score	MW	Accession
Scan(s)	P (pep)	XC	Sp	RSp
glucose phosphate isomerase	5.55E-15	30.22	63107.3	18201905
glyceraldehyde-3-phosphate dehydrogenase	7.77E-15	90.27	36030.4	7669492
glutathione transferase	4.88E-14	30.25	23341.0	4504183
transketolase isoform 1	1.13E-11	60.22	67834.9	4507521
mitochondrial ATP synthase beta subunit precursor	1.50E-11	20.19	56524.7	32189394
mitochondrial malate dehydrogenase precursor	2.09E-11	20.22	35480.7	21735621
aldo-keto reductase family 1, member B10-like	1.39E-10	20.20	36513.8	122937516
aldehyde dehydrogenase 1A1	1.48E-10	70.23	54827.0	21361176
aldo-keto reductase family 1, member B10	1.71E-10	50.22	35996.9	223468663
triosephosphate isomerase 1 isoform 1	3.56E-10	60.21	26652.7	4507645
glutathione reductase	8.98E-10	10.14	56221.0	50301238
solute carrier family 25 (mitochondrial carrier), member 31	8.67E-10	10.18	34999.4	13775208
translocase of inner mitochondrial membrane 50 homolog	8.74E-09	10.18	50433.2	48526509
ATP synthase, H+ transporting, mitochondrial F1 complex	1.98E-08	30.16	59713.7	4757810
acyl-Coenzyme A oxidase 1 isoform a	8.92E-08	10.16	74620.2	30089972
glucose-6-phosphate dehydrogenase isoform b	9.02E-08	50.18	59219.1	108773793
aldo-keto reductase family 1, member C2	1.04E-07	30.20	36712.0	4503285
NAD(P)H menadione oxidoreductase 1, isoform a	2.65E-07	40.18	30848.0	4505415
dehydrogenase/reductase member 2 isoform 1	5.10E-07	20.18	31475.6	33667109
thioredoxin	9.61E-07	20.18	11729.7	50592994
aldehyde dehydrogenase 3A1	1.98E-06	40.17	50362.9	206597439
peroxiredoxin 1	7.00E-06	20.17	22096.3	4505591
ATP synthase, H+ transporting, mitochondrial F0 complex	1.33E-05	10.15	7928.3	6005717
peroxiredoxin 6	5.07E-05	10.12	25019.2	4758638
NADH dehydrogenase 1 alpha subcomplex, 4, 9kDa	1.97E-05	10.17	9363.9	4505357

B

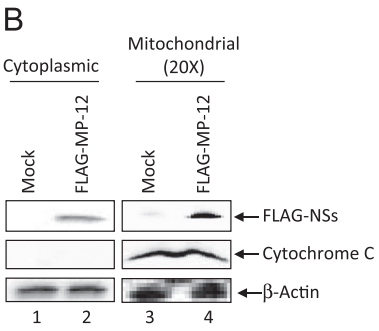

Fig. 4. NSs is associated with the mitochondria of infected cells. (A) Flag-NSs-MP-12 virus was used to infect HepG2 cells. Total cell lysates were immunoprecipitated with an antibody against the Flag tag and subjected to LC-MS/MS analysis. (B) Crude mitochondrial preparations were obtained from Flag-NSs-MP-12 infected HepG2 cells. Total cytoplasmic protein was maintained as controls. All lysates were analyzed by western blot for Flag (NSs), cytochrome C and actin. For the western blot analysis, a mitochondrial pellet from approximately 10^7 cells was used. For the cytoplasmic component, 1/5th of protein from 10^7 cells was used. This difference in relative protein utilized is indicated as 20X in the figure.

peptides identified about 183 proteins that were distinct from the IgG control immunoprecipitation. The 183 proteins covered a wide range of cytoplasmic proteins including metabolic enzymes, cytoskeletal proteins, chaperones, translational proteins including ribosomal components in addition to about 23 proteins that were associated with maintenance of oxidative homeostasis (Fig. 4A, Supplemental Table). We also observed a limited set of nuclear proteins including chromosome maintenance complex proteins, nuclear phosphoprotein, ras-related nuclear protein, RAN binding protein, nucleophosmin and nucleolin (Supplemental Table). The cytoplasmic components were in excess in this case because we had performed the immunoprecipitation with total protein lysates without enriching for nuclear proteins. Our focus was on the association of NSs with oxidative metabolism and we observed that many proteins including members of the mitochondrial F0 and F1 complex co-precipitated with the Flag-tagged NSs as shown by MS results. Next, we isolated mitochondria to determine if NSs can be detected in the mitochondrial fraction of infected cells at early time points. HepG2 cells were infected with the Flag-NSs-MP-12 virus and crude mitochondrial extracts were prepared at approximately 6 h post infection. The mitochondrial preparations were then lysed and western blots carried out using antibodies to the Flag tag and cytochrome C, a mitochondrial marker protein (Fig. 4B). Cytoplasmic fractions of the same preparations were run alongside as controls. Results demonstrated the inclusion of Flag-NSs in the mitochondrial fraction (Fig. 4B, lane 4) of Flag-NSs-MP-12 infected cells. Cytochrome C was detected in both mock-infected and Flag-NSs-MP-12-infected mitochondria (lanes 3, 4) as expected. Finally, β-actin was probed as a control and observed in all samples. Therefore, our results suggest that the viral protein NSs may be included in the mitochondria of infected cells at earlier time points after infection which may contribute to the NSs-dependent oxidative stress phenotype at early time frames.

To further elucidate the relationship of NSs with the host mitochondria we performed confocal microscopy. Briefly, HepG2 cells were transfected with FLAG_NSs, fixed after 6 h and stained with antibodies against the FLAG tag and mitochondria. Fig. 5A shows representative images of HepG2 cells positive for FLAG_NSs and displaying co-localization with mitochondria. In Fig. 5A, we demonstrate the colocalization of NSs with the mitochondria as observed in a Z-stack section of the image in the last panel (expanded inset). A total of 211 cells were visualized and counted of which 128 were positive for FLAG_NSs. Of the 128 cells, 44 cells showed co-localization of the FLAG_NSs and the mitochondria (as inferred by the yellow staining pattern). Additional examples of colocalization of NSs and mitochondria in infected HepG2 cells are shown in Fig. 5B. We also confirmed expression of FLAG-NSs at the 6 h time point by performing a western blot for FLAG-NSs in infected cells. The data shown in Fig. 5C indicates that FLAG-NSs could be detected in these cells at the 6 h time point. Finally, we asked the question whether NSs, by itself, out of context of a viral infection would localize to the mitochondria. To answer that question, we transfected a plasmid encoding FLAG-NSs into HepG2 cells. Twenty-four hours post transfection, the cells were fixed and stained with anti-FLAG and anti-mitochondria antibodies and observed by confocal microscopy. NSs showed a diffuse nuclear staining and no distinct filaments could be detected as in the case

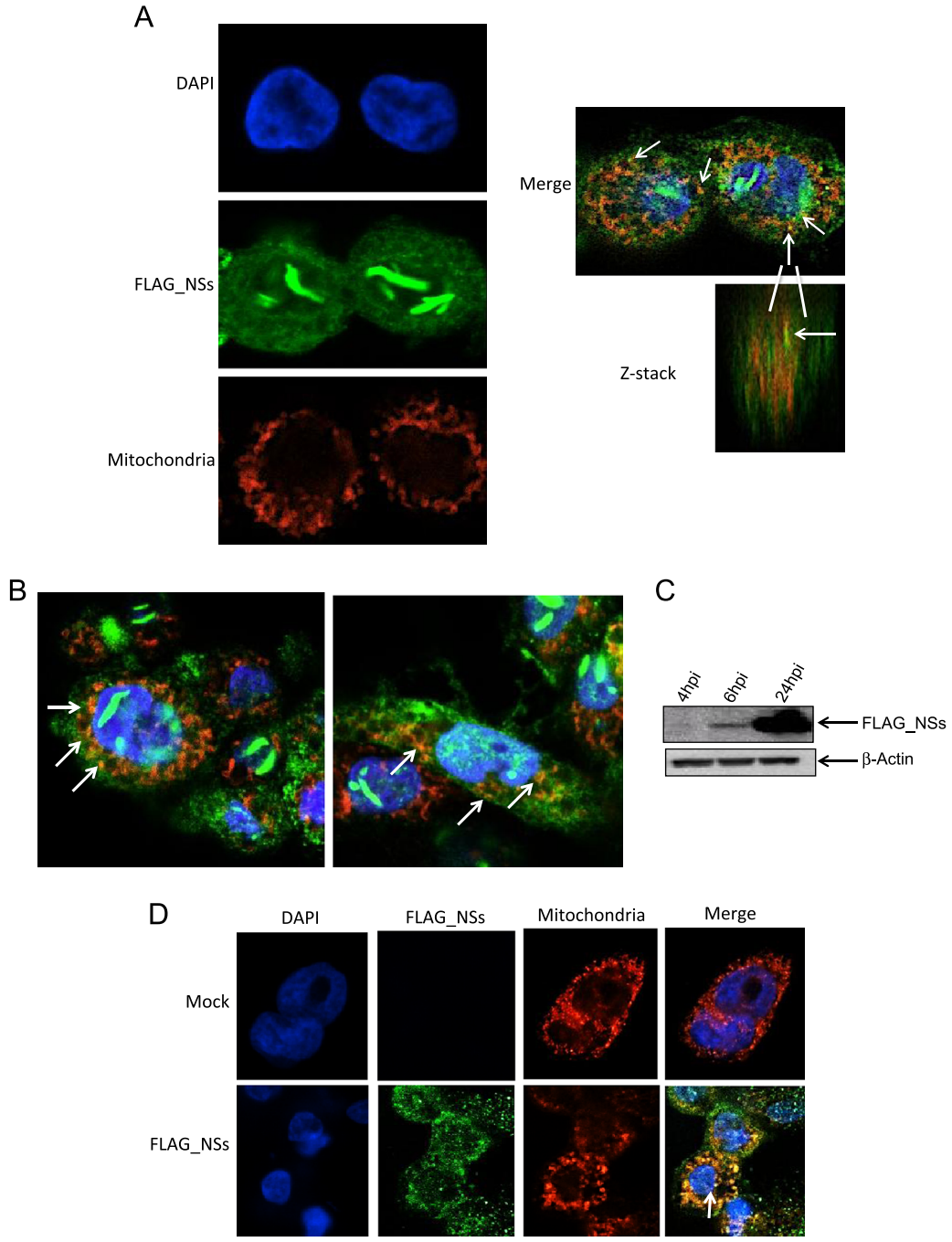

Fig. 5. NSs co-localizes with mitochondria. HepG2 cells were infected with FLAG_NSs-MP-12 and cells were fixed after 24 h and stained with antibodies against the FLAG tag and mitochondria (α-Tomm20). Images of stained cells were obtained by confocal microscopy. Representative images of HepG2 cells positive for FLAG_NSs displaying co-localization with mitochondria are shown in A and B. Co-localization of FLAG_NSs with the mitochondria is indicated by the arrows. The co-localization was confirmed by Z-stack analysis. A total of 211 cells were visualized and counted of which 128 were positive for FLAG_NSs. Of the 128 cells, 44 cells showed co-localization of the FLAG_NSs and the mitochondria (as inferred by the yellow staining pattern). (C) HepG2 cells were infected with FLAG_NSs-MP-12 (MOI: 3) and at 4, 6 and 24 h post infection cell lysates were collected and protein extracted as described in the materials and methods section. Cell lysates were resolved by SDS-PAGE and western blots carried out using anti-FLAG and anti-β-actin antibodies. (D) HepG2 cells were transfected with FLAG_NSs plasmid (1 μg) and 24 h post transfection cells were fixed and stained with anti-FLAG and anti-Tomm20 antibodies. Images of stained cells were obtained by confocal microscopy. Representative images of HepG2 cells positive for FLAG_NSs displaying co-localization with mitochondria are shown in D. Co-localization of FLAG_NSs with the mitochondria is indicated by the arrows.

of a MP-12 infection. However, strong colocalization with mitochondria was evident in multiple FLAG-positive cells (Fig. 5D) suggesting that NSs, out of context of a viral infection, could localize to mitochondria in HepG2 cells. Cumulatively, our mass spectrometry studies, mitochondrial enrichment studies and confocal studies indicate that at least a fraction of the cytoplasmic NSs localized in the mitochondria in infected cells.

Activation of the NFkB response and p53 response accompanies oxidative stress in RVFV-infected liver cells

ROS has been shown to be involved in host responses to invading pathogens by functioning as secondary signaling messengers (Waris et al., 2001; Gwinn and Vallyathan 2006; Yang et al., 2010; Imai et al., 2008). One such host-signaling event that is

modulated by intracellular ROS levels is the NFkB pathway. Earlier studies performed using MP-12 infected epithelial cells have shown the activation of the NFkB cascade at early time points following infection (Narayanan et al., 2012). Therefore, we asked whether the activation of NFkB components can be temporally correlated with an increase in ROS in MP-12 infected liver cells. To address this question, we determined whether nuclear translocation of p65 can be observed at early and late time points after infection of HepG2 cells with wild type MP-12 or UV-MP-12. We determined that the UV-inactivation procedure rendered the virus replication incompetent by plaque assays (data not shown; (Narayanan et al., 2012)). Mock infected cells were included as controls. Additionally, we infected cells with the MP-12ΔNSs mutant virus to evaluate the effect of NSs on the nuclear translocation of p65. Infected cells were fixed at 1 h post infection, stained with anti-p65 antibody and visualized by confocal microscopy. We observed significant nuclear translocation of p65 following infection with MP-12 as indicated in Fig. 6A (MP-12 panel). In the case of infection by UV-MP-12, we did not observe significant localization of p65 in the nucleus and did not look different from the mock infected cells. However, in the case of MP-12ΔNSs, we observed a partial localization of p65 in the

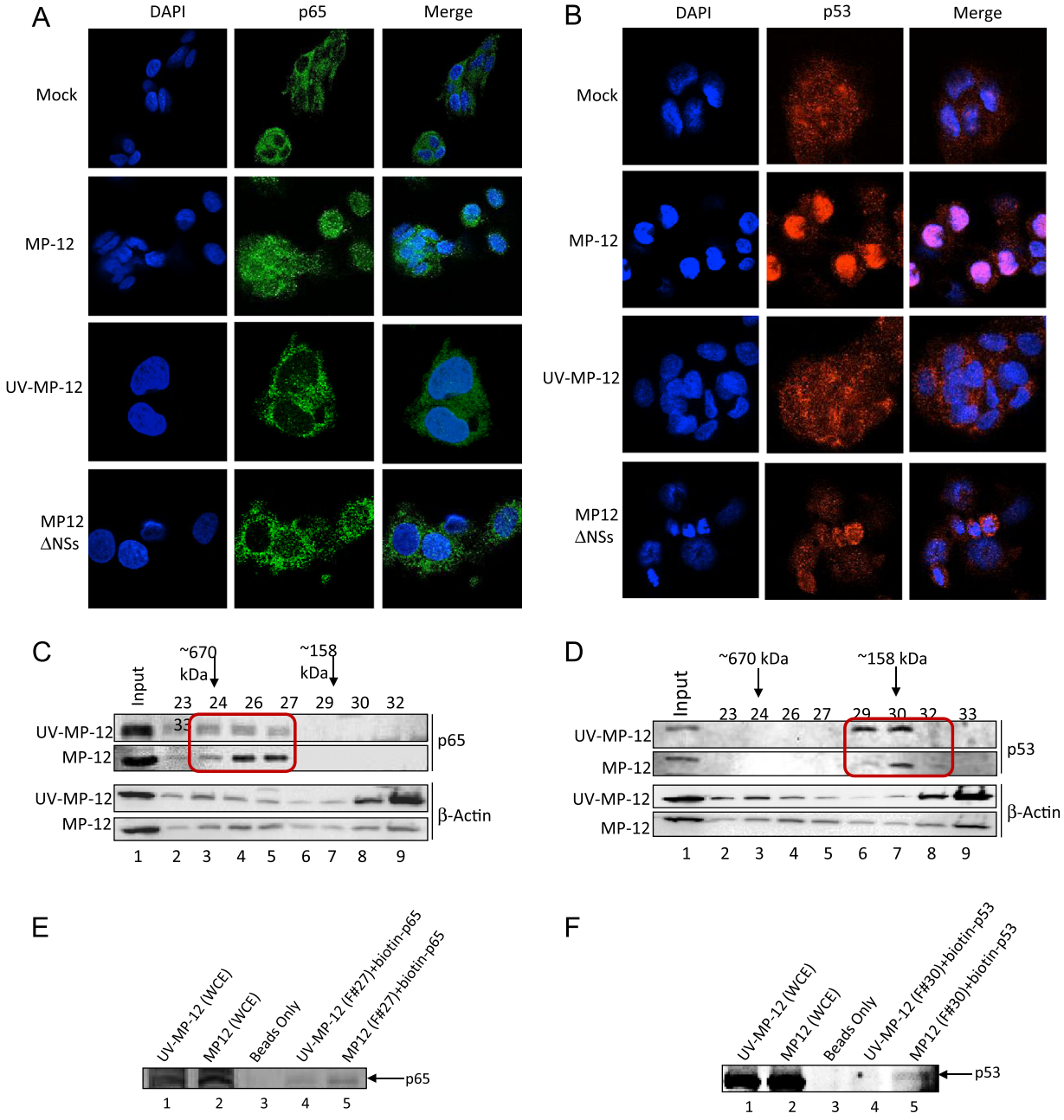

Fig. 6. Activation and macromolecular reorganization of p65 and p53 complexes in MP-12 infected cells. (A) and (B) Nuclear translocation of p65 and p53 was determined by confocal microscopy. MP-12, UV-MP-12, MP-12ΔNSs (MOI: 3) or mock infected HepG2s were fixed at 1 and 24 h post infection and stained with anti-p65 (total) and anti-p53 (total) antibody respectively and DAPI. (C) and (D) MP-12 and mock infected HepG2 cells (MOI: 10) were lysed and total protein lysates (2 mg) were size fractionated using a Superose 6 h 10/30 size-exclusion chromatography column using the AKTA purifier system. About 50 fractions were obtained from each sample. Protein from every alternate fraction spanning a size range between 1 mDa and 100 kDa was precipitated and analyzed by western blotting using anti-p65 (total), anti-p53 (total) and anti-β-actin antibodies. The red squares in the p65 blot (panel C) and p53 blot (panel D) show reorganized p65 and p53 complexes that eluted in MP-12 infected samples compared to mock infected cells. (E) and (F) Fractions 27 and 30 from UV-MP-12 and MP-12 infected lysates were utilized in a DNA binding assay using Biotin-coupled oligonucleotide probes with binding sites to p65 and p53 respectively. The lysates were then incubated with streptavidin beads and incubated at 4 °C. The beads were then washed, proteins eluted and analyzed by western blot for p65 and p53 binding.

nucleus in some cases while the number of cells that were positive for nuclear p65 was more in the case of MP-12 infected cells (Fig. 6A). We also analyzed the phosphorylation status of p65 and IκBα as a reflection of NFkB activation after MP-12 infection by western blot analysis, which indicated an increased phosphorylation of p65 on Serine 536 and IκBα on Serine 32 (data not shown). Cumulatively, our experiments demonstrated activation of the NFκB cascade at early time points following RVFV infection.

A second signaling response that is activated by intracellular ROS is DDR, due to damage to nuclear and mitochondrial DNA. Previous studies have demonstrated that RVFV infection activates both DDR and p53 in epithelial cells at later time points in infection even though no significant damage to DNA could be detected (Baer et al., 2012; Austin et al., 2012). In order to determine if similar responses operate in liver cells following RVFV infection, we determined nuclear translocation of p53 at late time points after MP-12 infection. Accordingly, HepG2 cells were infected with either MP-12 or UV-MP-12, stained with anti-p53 antibody (total p53) and imaged by confocal microscopy. Mock infected cells and MP-12ΔNSs infected cells were maintained as controls. Results revealed that in the case of MP-12 infection, nuclear p53 can be readily detected in multiple cells while in the case of infection by the UV-inactivated virus p53 was more widely and diffusely distributed in the cell with no apparent nuclear enrichment (Fig. 6B). In the case of MP-12ΔNSs, we observed occasional nuclear p53 while the number of cells positive for nuclear p53 was significantly higher in the case of MP-12 infected cells. We analyzed the phosphorylation status of p53 and DDR associated proteins Chk2 and H2AX by western blots and observed higher levels of phosphorylation of p53 on Serine 15 and Serine 392 in MP-12 infected cells than UV-MP-12 infected cells (data not shown). Similarly, we noted that Chk2 and H2AX were also phosphorylated to a greater extent in MP-12 infected cells when compared with cells infected with UV-MP-12 with no significant changes in total levels of H2AX and Chk2 (data not shown). Cumulatively, these observations in liver cells mirror earlier observations in epithelial cells in that RVFV infection activates DDR and p53 signaling following infection. As these responses have been observed to occur in different cell types at later time points following infection, we suggest that RVFV infection-triggered ROS induces the NFκB signaling cascade at early time points and the activation of DDR and p53 responses at later time points after exposure.

Macromolecular reorganization of p65 and p53 occurs in RVFV-infected liver cells.

Activation of fundamental innate immune responses including activation of p65 and p53 often involves reorganization of a macromolecular complex from an inhibitory configuration to one that is activating. Prior experiments that focused on multiple host kinases that influence host innate immune response including the IKK complex (IKK-β), GSK-3β and Cyclin T/Cdk9 demonstrated macromolecular reorganization of these kinase complexes in response to viral infections (Narayanan et al., 2012a, 2012b; Kehn-Hall et al., 2012). Typically, the reorganization of these kinases resulted in the appearance of novel, small molecular weight species as observed by size fractionation column chromatography approaches (Narayanan et al., 2012a, 2012b; Kehn-Hall et al., 2012). Based on prior evidence that viral infections induced formation of novel, functional macromolecular complexes, we asked whether p65 and p53 displayed any alterations in their size fractionation profiles that may correlate with their activation status. We addressed the issue by performing column chromatography using whole cell lysates that were obtained from HepG2 cells infected with MP-12 and UV-MP-12. We carried out chromatography separation using a Superose 6 sizing column and analyzed fractions that were between the ~800 kDa and 100 kDa range for distribution patterns of p65 and p53. β-actin was analyzed as a control in both cases to monitor for presence of protein in the analyzed fractions. We observed that in UV-MP-12 infected cells, p65-containing complexes showed a wider distribution range from approximately 800 kDa to about 300 kDa (Fig. 6C, lanes 2–5). In the case of MP-12 infected cells, we noticed a decrease in the high-molecular weight complexes (670 kDa and above; lanes 2 and 3) and an increase in the p65-containing complexes in the 300 kDa range (670 kDa and below; lanes 4 and 5). This reorganization of the p65 complexes was not due to changes in total p65 protein levels as revealed by comparable p65 in the input lanes in the MP-12 and UV-MP-12 lysates (lane 1). Similarly, we observed that in UV-MP-12 infected cells, p53 was predominantly observed between the 200 and 150 kDa range (Fig. 6D, lanes 6 and 7). In the case of MP-12 infected cells, p53 appeared to have a more stream-lined, narrow distribution where the majority of the higher migrating form that was visible in the UV-MP-12 infected samples (lane 6) disappeared while p53 was concentrated in the 150–100 kDa range (lane 7, 8).

As a next step, we determined whether the low molecular weight versions of p65 and p53 that were observed in MP-12 infected cells were functionally competent to bind appropriate promoter sequences and how the binding of the low molecular weight forms compared to the forms that existed in UV-MP-12 infected cells. To answer that question, we performed DNA binding studies using fractions 27 and 30 from MP-12 and UV-MP-12 infected cell lysates using biotin labeled p65 and p53 oligonucleotides (Furia et al., 2002). The experiment was carried out by incubating fractions 27 and 30 with the appropriate biotin-oligonucleotides. Twenty-four hours later, streptavidin beads were added and incubated at 4 °C for a few hours. The beads were then washed twice with high salt buffer, bound proteins eluted and analyzed by western blot using anti-p65 and anti-p53 antibodies. Our results demonstrated that for p65, more protein was bound to the oligonucleotide when fraction 27 from MP-12 infected lysate was used as compared to UV-MP-12 infected cells (Fig. 6E). Similarly, in the case of p53, we observed an increased binding of p53 to the corresponding oligonucleotide when the fraction was obtained from MP-12 infected cells (Fig. 6F). Collectively, the DNA binding studies performed with the low molecular weight complexes of p65 and p53 were suggestive of the possibility that these versions of p65 and p53 obtained from MP-12 infected cells may be more efficient in binding to DNA than those present in the UV-MP-12 counterparts.

Cumulatively, based on size fractionation of p65 and p53-containing complexes in MP-12 infected cells, we observe reorganization of both proteins that correlate with a productive infection. The reorganization of both proteins primarily pointed towards appearance of low molecular weight species in the case of MP-12 infection and the low molecular weight proteins displayed efficient DNA binding.

RVFV infection of liver cells results in increased NFκB and p53 induced gene expression

One of the well-documented consequences of NFκB activation in response to upstream stimuli such as viral infection and ROS is the increased expression of inflammatory cytokines that play integral roles in downstream effects including the onset of apoptosis and pathological outcomes. Mouse model studies have demonstrated modulation of inflammatory gene expression in the liver of RVFV infected animals, drawing connections between inflammatory gene responses and hepatitis (Smith et al., 2010; Ding et al., 2005). Therefore, we asked whether MP-12 infection resulted in NFκB-induced alteration of cytokine expression in liver cells. We looked at IL8 expression in infected HepG2 cells as a

representative of inflammatory mediator expression. We chose IL8 as a candidate for analysis because IL8 is a potent chemoattractant and is associated with inflammatory gene expression in multiple liver-associated disease phenotypes including HCV infection (Polyak et al., 2001a, 2001b). HepG2 cells were infected with MP-12 and total RNA was isolated at 24 h post infection. We performed a RT-PCR assay with IL8 primers to determine changes in IL8 expression. GAPDH expression was analyzed alongside as a control. We observed a strong increase in IL8 expression at 24 h post infection (Fig. 7A). To quantitatively analyze IL8 expression in MP-12 infected cells in comparison with either mock infected or UV-MP-12 infected cells, we performed qRT-PCR using RNA obtained at 24 h post infection. Levels of 18s rRNA were used to normalize the IL8 expression numbers and the results indicated that MP-12 infection resulted in a robust increase in IL8 expression (Fig. 7B). To compare with the increase in gene expression, we also determined secreted IL8 protein in the supernatants of infected cells. As the viral protein NSs is known to suppress the innate immune inflammatory response, we performed ELISAs to compare IL8 levels in the supernatants of MP-12 infected HepG2 cells with those infected with the NSs and NSm mutant viruses. As expected, we observed an increase in IL8 in the supernatants of MP-12 infected cells when compared to the mock-infected control. In the case of the NSs mutant, there was more IL8 in the medium when compared to MP-12 infected cells while the NSm mutant did not influence IL8 secretion significantly (Fig. 7C, left panel).

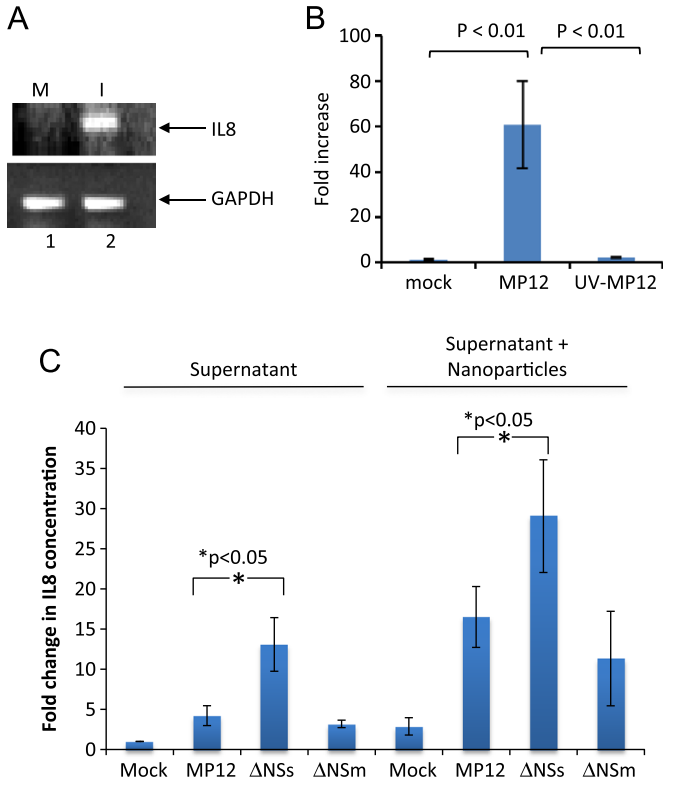

Fig. 7. NFκB mediated cytokine expression and p53 mediated proapoptotic gene expression are increased in MP-12 infected cells. (A) MP-12 (I) and mock infected (M) cells were lysed at 24 h post infection and total RNA was isolated. The expression of IL8 was determined by RT-PCR with IL8 specific primers. GAPDH expression was determined using GAPDH-primers as a control. (B) MP-12, UV-MP-12 infected cells and mock infected cells were lysed at 24 h post infection and qRT-PCR was performed with primers to IL8. 18sRNA expression levels were used to normalize IL8 levels. (C) Supernatants from MP-12, MP-12ΔNSs and MP-12ΔNSm infected cells were obtained at 24 h post infection and analyzed by ELISA for IL8 protein. In the left panel, all supernatants (100 μl per sample) were analyzed without any kind of enrichment. In the right panel, 8 ml of supernatant from each infection was incubated with hydrogel nanoparticles (cibacron blue bait and VSA shell) for 1 h at room temperature, the particles spun down by high speed centrifugation (10,000 rpm for 15 min) and contents eluted in water (100 μl). ELISA was then performed using the entire eluted volume for presence of IL8 protein.

In order to analyze differences in the amounts of IL8 in the media in a more sensitive manner, we utilized hydrogel nanoparticles that have been demonstrated to successfully capture and enrich low molecular weight analytes. The captured analytes can be subsequently detected by conventional methods such as ELISA (Tamburro et al., 2011; Longo et al., 2009; Fredolini et al., 2008). Analyte capture is mediated by specific chemical baits incorporated into the nanoparticles and the capture efficiency is enhanced by the porosity of the particle that permits size sieving. Specifically, the nanoparticles have been demonstrated to capture and preserve IL8 from enzymatic degradation (Tamburro et al., 2011). Supernatants from MP-12 infected cell cultures and NSs and NSm mutant virus infected cultures were incubated with hydrogel nanoparticles (with a cibacron blue bait and a VSA shell) for 1 h after which the particles were pelleted and bound IL8 eluted. The eluted protein was then analyzed by ELISA to obtain more sensitive and quantitative differences in IL8 secretion. Accordingly, we observed >3-fold increase in IL8 protein secreted in the culture supernatant of MP-12 infected liver cells over control. More elevated levels of IL8 could be detected in the supernatants of cells infected with NSs mutant virus while the NSm mutant virus actually resulted in lower levels of IL8 in the media when compared to MP-12 infection (Fig. 7C, right panel). Therefore, our data suggests that MP-12 infection of liver cells results in both increased IL8 gene expression and protein expression levels.

Treatment with antioxidants reversed the observed phenotypic phenomena associated with MP-12 infection

We reasoned that if the observed increase in superoxide levels in MP-12 infected cells contributed to the down stream effects including activation of p65 and p53, activated expression of inflammatory mediators, and activated expression of apoptosis associated genes and increased apoptosis, controlling increase in superoxide at early time points of infection by antioxidants should reverse those phenotypic endpoints. We first checked if treatment of HepG2 cells with a well-documented antioxidant, curcumin, decreased superoxide levels in infected cells. HepG2 cells were pretreated with curcumin (1 μM) for 1 h and then infected with MP-12. Cells were stained with MitoSox at 3 h post infection and analyzed by confocal microscopy, which showed a marked decrease in intracellular superoxide levels (Fig. 8A).

As a next step, we determined if controlling early induction of superoxide by curcumin inhibited nuclear translocation of p65 at early time points and p53 at later time frames following infection. HepG2 cells were pretreated with curcumin (1 μM) and infected with MP-12 virus. Infected, untreated cells and mock infected cells were maintained as controls. Cells were fixed at 1 h post infection and stained for p65 localization (Fig. 8B). The results demonstrated that pretreatment of HepG2 cells with curcumin decreased nuclear localization of p65 in infected cells. We performed a similar experiment to determine the consequence of pretreatment with antioxidants on nuclear migration of p53 at later time frames in MP-12 infected cells. Results followed a similar pattern to p65, indicating a decreased nuclear migration of p53 (Fig. 8B).

We then determined whether pretreatment of cells with the antioxidant attenuated expression of inflammatory mediators. We isolated total RNA from cells infected with the MP-12 virus or the UV-MP-12 virus at 24 h post infection, and RNA was also isolated from untreated cells and curcumin treated cells. We performed qRT-PCR for multiple cytokines including IL2, IL4, IL6 and IL8 and noticed that pretreatment with the antioxidant robustly down regulated inflammatory gene expression. Curcumin has a long standing record of being an anti-inflammatory molecule (Zhang

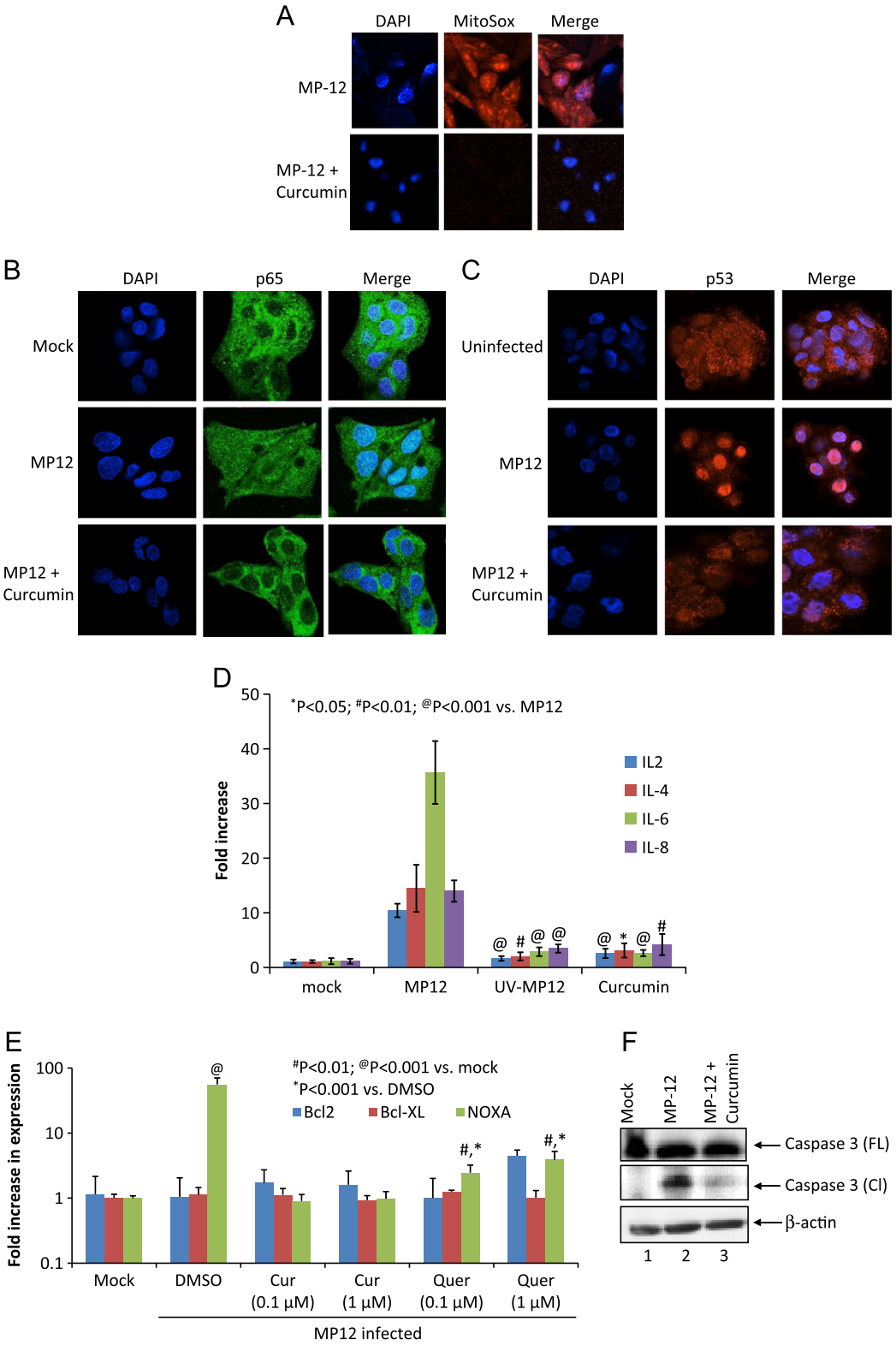

Fig. 8. Antioxidants reverse apoptotic and cytokine gene expression, decrease apoptosis and viral multiplication in infected cells. (A) HepG2 cells were either infected with MP-12 (MOI: 3) or pretreated with curcumin (1 μM) and then infected with MP-12 (MOI: 3). Cells were stained with Mitosox and DAPI and imaged by confocal microscopy. (B) and (C) HepG2 cells were either mock infected, MP-12 infected or pretreated with curcumin (1 μM) and then infected with MP-12 (MOI: 3). Cells were fixed at 1(B) and 24 (C) hours post infections and stained for p65 and p53 respectively and DAPI. (D) HepG2 cells were mock infected, MP-12, UV-MP-12 infected or pretreated with curcumin (1 μM) and then infected with MP-12 (MOI: 3). Levels of IL2, IL4, IL6 and IL8 were quantified by qRT-PCR and are represented graphically. (E) HepG2 cells were pretreated with curcumin and quercetin (0.1 and 1 μM) for 2 h, infected with MP-12 virus or mock infected and post treated with the antioxidants for up to 24 h. Cells treated with DMSO alone were maintained as controls. Total RNA was obtained and analyzed by qRT-PCR with primers against Bcl2, Bcl-XL and NOXA. (F) HepG2 cells were either mock, MP-12 infected or pretreated with curcumin and then infected with MP-12. Total protein was resolved by SDS-PAGE. Western blot was performed with antibody against caspase 3 (recognizes both cleaved [Cl] and full length [FL] forms. Fold change in intensities of the 11 kDa cleavage product is indicated at the bottom. B-Actin served as a loading control.

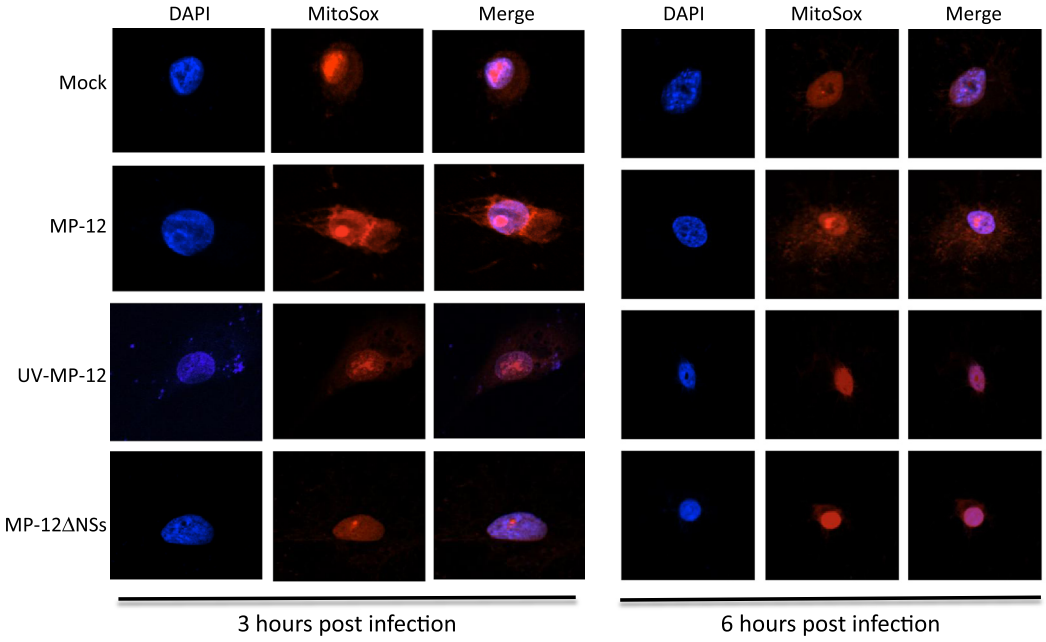

Fig. 9. ROS activation in MP-12 infected human primary hepatocytes. Human primary hepatocytes were either mock, MP-12, UV-MP-12 or MP-12ΔNSs infected (MOI: 3). Three (A) and 6 (B) hours post infection hepatocytes were stained with MitoSox and DAPI and imaged by confocal microscopy.

et al., 2011; Aftab and Vieira, 2010; Jackson et al., 2006) and our current result reproduced that trend (Fig. 8D). We also looked at the expression of genes associated with the onset of apoptosis that were regulated by p53 and p65 in the presence of curcumin. Total RNA from MP-12 and UV-MP-12 infected cells was obtained and analyzed by qRT-PCR with primers against pro- and anti-apoptotic genes including Bcl2, Bcl-XL, and Noxa. The most prominent change in gene expression was observed for Noxa, which agrees with our earlier published data although those studies were done in epithelial cells (37). This increase in Noxa expression can be observed in the sample marked DMSO which actually refers to MP-12 infected cells which were treated with the DMSO control (Fig. 8E). In the case of infected cells, which were treated with increasing concentrations of curcumin or Quercetin, another antioxidant (Zhang et al., 2011; Aftab and Vieira 2010; Jackson et al., 2006), the Noxa expression levels decreased (Fig. 8E). In the case of quercetin, we noticed that in addition to down regulating Noxa, there was an increase in the expression of Bcl-2 in treated cells, thus alluding to the onset of an anti-apoptotic phenotype.

Finally, we asked whether these observed changes in p65 and p53 localization and alteration of inflammatory and apoptotic gene expression by antioxidant treatment reflected as reduced apoptosis of infected cells. To answer this question, we performed western blots to determine caspase 3 cleavage as a marker of apoptosis. MP-12 infected, untreated cells were compared with MP-12 infected, curcumin treated cells and mock infected cells. The results suggested that pronounced cleavage of caspase 3 could be observed in the MP-12 infected cells but that it was reduced in the presence of the antioxidant (Fig. 8F).

Cumulatively, our data suggested that pretreatment of MP-12 infected HepG2 cells with an antioxidant lowered the levels of reactive superoxide during the early stages of the infectious process, which reflected as reduced activation of p65 and p53, reduced inflammatory and apoptotic gene expression, and, finally, reduced apoptosis.

MP-12 infection of primary hepatocytes resulted in induction of reactive superoxide species

We wanted to determine if the changes relevant to NSs-dependent superoxide increase in MP-12 infected HepG2 cells recapitulated in a primary hepatocyte cell system. To address this question, primary hepatocytes were infected with MP-12, UV-MP-12 and MP-12ΔNSs viruses. Mock infected cells were maintained as controls. Cells were plated in eight chambered collagen coated glass slides, infected with the virus strains (MOI:3) and stained with MitoSox at 3 h and 6 h post infection. Microscopic observation indicated that in the case of all viral exposures a strong nuclear signal was observed at the early time point and that at the 6 h time point the mock infected cells also showed intense nuclear staining. This led us to conclude that the nuclear staining phenomenon may be a nonspecific event in the case of primary hepatocytes (Fig. 9A and B). However, at both the 3 and 6 h time points, we noticed intense cytoplasmic staining in the case of MP-12 infected cells while this phenotype could not be observed in the case of UV-MP-12 infected and MP-12ΔNSs infected cells. Cumulatively, the data suggested that a NSs mediated early increase of superoxide species in MP-12 infection can be observed in primary hepatocytes.

Discussion

RVFV infections have often been associated with pronounced liver damage with in vivo evidence indicating apoptosis of liver cells (Smith et al., 2010, 2012; Ding et al., 2005). The exact mechanisms that contribute to the liver damage in the face of RVFV infection is however unclear. Our previous publications that have investigated host response to RVFV infection have indicated that multiple host phospho-signaling pathways exert a strong influence on the apoptotic versus antiapoptotic environment of the cell (Popova et al., 2010). We had demonstrated that both NFκB and p53-based signaling responses were activated during infection in the case of lung epithelial cells and these signaling responses were necessary for viral replication (Baer et al., 2012; Narayanan et al., 2012; Austin et al., 2012). An upstream event that is known to influence both NFκB and p53 responses is oxidative stress. We had shown that RVFV infection increased the levels of expression of superoxide dismutase 1 (SOD1), and activated p38 MAPK-based stress responses (Narayanan et al., 2011). Therefore, prior data suggested that increase in ROS may be an important

component in pathology associated with RVFV infection, thus prompting the question of whether increased ROS may play a role in the observed apoptosis of liver cells. To test this possibility, we directly determined ROS levels in MP-12 infected HepG2 cells at early time points after infection. Our data indicated that there was an increase in MitoSox fluorescence (reflective of intracellular ROS) in infected cells over uninfected cells at 3 h post infection (Fig. 1). In the absence of the viral protein NSs, we noticed decreased MitoSox staining at early time points after infection (Fig. 2A, B) while this effect disappeared at later time points (Fig. 2C, D). This suggested that the involvement of NSs in oxidative stress responses may be more pronounced at early time points while at later time points additional viral and host components may be involved in the increase in intracellular ROS.

Our data demonstrates that NSs may be associated with components of the mitochondria in infected cells (Figs. 3 and 4). This observation could explain the decreased ROS detected at early time points with the NSs mutant virus. Many studies have demonstrated association of viral proteins with the mitochondria and the resultant effect on host response to an infection. A recent report by Terasaki et al. has demonstrated that the C-terminal region of the antiapoptotic NSm protein of RVFV may target NSm to the mitochondria of infected cells and this may be related to the antiapoptotic phenotype observed with the NSm mutant virus (Terasaki et al., 2013). HCV proteins have also been demonstrated to target the mitochondria and cause alteration of mitochondrial function that contributes to potent imbalances in the redox potential resulting in oxidative stress induced inflammation (Piccoli et al., 2007). NSs, by its association with the F0 or F1 complex of the mitochondria, could influence early increase in intracellular ROS levels by disrupting the electron transport chain. The disruption can occur either because of a functional compromise of key subunits such as NADPH oxidase, or due to ion imbalances such as calcium influx into the mitochondria or both. Both of these events have been known to occur due to virus protein-mediated mitochondrial disruption that results in increased intracellular ROS due to disruption of the mitochondrial electron transport machinery (Piccoli et al., 2007; Korenaga et al., 2005).

A delicate balance of the intracellular ROS level is an important requirement for the maintenance of cell homeostasis. However, the adverse effect of unregulated intracellular ROS is that these reactive species would nonspecifically oxidize many essential cellular macromolecules resulting in acute damage to the cell and disruption of essential cellular functions. Persistent imbalance in ROS in spite of cellular antioxidant mechanisms is indicative of breakdown of regulatory mechanisms that often culminate in apoptosis. ROS, therefore, also acts as a secondary messenger to activate many host signaling responses, including NFkB and p53 (Gong et al., 2001; Waris et al., 2001; Gwinn and Vallyathan, 2006). Consequently, we asked whether p65 (a key effector protein of the NFkB signaling cascade) and p53 were activated in infected liver cells. Our experiments demonstrated that both p65 and p53 are localized to the nucleus in liver cells infected with RVFV (Fig. 6A, B).

One of the hallmarks of NFκB activation and prerequisite for p65 translocation to the nucleus is a reorganization of the p65-containing complex in the cytoplasm. p65 is retained in the cytoplasm as a complex with the inhibitory IκBα protein. A central kinase of the NFκB cascade is the IκB kinase complex (IKK) that phosphorylates IκBα, which is then proteomically degraded. This releases p65, which then associates with p50 and translocates to the nucleus where it binds κB elements on select sets of genes and activates transcription. Our earlier studies have demonstrated that viral infection led to profound alterations of multiple host regulatory components including kinases that influenced viral multiplication and pathological outcomes in the host (Narayanan et al., 2012a, 2012b; Kehn-Hall et al., 2012; Ramakrishnan et al., 2012). We reasoned that p65 would be reorganized in these cells as IκBα would be phosphorylated and degraded. To determine if this occurred in RVFV infected liver cells, we fractionated cell lysates using size fractionation chromatographic methods and analyzed p65 distribution based on size. Our data revealed that p65 which showed a wide distribution range from ~800 kDa to 500 kDa in mock infected cells was restricted to a much narrower range closer to ~670 to 500 kDa in RVFV infected cells (Fig. 6C). When we tested for p53 distribution in a similar manner, we made comparable observations in that p53 in infected cells was restricted to a narrower size range than in mock infected cells, although the observed shift was relatively modest when compared to p65 (Fig. 6D). This reorganization of p65 and p53 in infected cells to smaller-sized complexes may be attributed to removal of inhibitory proteins that would otherwise retain these transcription factors in the cytoplasm. Functionally, it is interesting to speculate that the lower molecular weight complexes may lack inhibitory components for promoter binding and therefore may be able to bind to promoters more easily and facilitate transcription. Our DNA binding studies using the low molecular weight versions of p65 and p53 supported this idea and we observed increased binding of both proteins with corresponding DNA sequences (Fig. 6E, F). It may be possible that the higher DNA binding property of these low molecular weight proteins is due to additional modifications such as phosphorylation or acetylation which may serve as intracellular switches that influence transcriptional regulation (Furia et al., 2002; Chen et al., 2001, 2002; Kim et al., 2012; Jain et al., 2012).

Induction of cytokine responses as a consequence of infection leads to inflammation in affected tissues. When we analyzed gene and protein expression profiles of inflammatory cytokines in liver cells following RVFV infection, we observed that IL8 expression was induced at both the gene and protein expression levels (Fig. 7). The connection between liver injury, apoptosis, IL8 and NFκB activation has been well established in the case of HCV infections where infection induced NFκB activation led to increased IL8 expression and apoptosis, as reflected by caspase 3 cleavage (Balasubramanian et al., 2005). Similarly, IL8 induction in liver cells following CCHF infection culminating in apoptosis has also been documented (Smith et al., 2012). Increased cytokines are connected with induction of apoptosis phenotypes in the liver and are often considered to be biomarkers of liver cytotoxicity (Komita et al., 2006; Sharma et al., 2005; Duran et al., 2004; Chalaris et al., 2007; Lacour et al., 2005). These cytokines induce intracellular signaling mechanisms such as STAT signaling that leads to apoptosis and hepatitis (Duran et al., 2004). We also observed a potent increase in the expression of p53-modulated Noxa gene expression at later time points of infection (data not shown). The increase in expression of Noxa was previously documented in epithelial cells following RVFV infection (Baer et al., 2012). Increase in expression of these inflammatory mediators and p53-responsive genes will contribute directly to the onset of apoptosis (Bantel and Schulze-Osthoff 2003; Tonino et al., 2011; Yee et al., 2011). Our data on ROS activation indicated that NSs mediated activation of ROS was an early event during the infectious process. However, ROS activation at a later time point proceeded regardless of NSs suggesting that additional events mediated the onset of oxidative stress at later time points.

In order to establish a link between the increase in ROS and increase in apoptosis inducing gene expression profiles, we treated HepG2 cells with increasing concentrations of free radical scavengers such as curcumin. We observed that pretreatment of infected cells with antioxidants reversed many of the deleterious outcomes of MP-12 infection including reduction of free superoxide species,

reduced activation of p65 and p53, reduced induction of inflammatory and apoptotic gene expression, and, finally, reduced incidence of apoptosis (Fig. 8). It is possible that decrease in apoptotic gene expression and proinflammatory cytokine production may be a result of decreased viral multiplication in the presence of antioxidants, as our previous manuscript had demonstrated that curcumin inhibits RVFV multiplication (Narayanan et al., 2012).

In conclusion, our data supports the idea that RVFV infection leads to increased ROS in infected liver cells that activates NFκB responses early in infection and p53 responses later in infection. These transcription factors in turn augment cytokine responses and pro-apoptotic gene expression in the infected cells that culminate in apoptosis mediated cell death. These sets of data provide compelling evidence for the use of antioxidants to achieve better hepatoprotection and possibly decrease pathogen multiplication in the case of RVFV infections, as in the case of HCV infection.

Materials and methods

Viruses and cell lines

The attenuated RVFV strain, MP-12 used in this study was obtained by 12 serial passages of the virulent ZH548 virus in the presence of 5-fluorouracil that resulted in a total of 25 mutations spanning the L, M and S segments of the viral genome (Vialat et al., 1997; Caplen et al., 1985). Other strains included are the MP-12ΔNSm strain and the MP-12ΔNSs. MP-12ΔNSm (arMP-12-del21/384) has a large deletion in the pre-Gn region of the M segment and as a result does not express NSm, 78 kDa, 75 kDa, or 73 kDa proteins encoded by this region (Won et al., 2007). MP-12ΔNSs (rMP-12-NSdel) completely lacks the NSs ORF (Ikegami et al., 2006). Flag-tagged NSs virus has a C-terminal Flag-tagged NSs inserted in place of NSs in the MP-12 backbone (Ikegami et al., 2009). MP-12 strain was inactivated by exposing virus to ultraviolet radiation and termed UV-MP-12 (Narayanan et al., 2012). Human liver fibroblast cells (HepG2 cells) were maintained in 50% DMEM, 50% Ham's F-12, 10% Fetal Bovine Serum (FBS), 1% Penicillin/Streptomycin and 1% L-Glutamine at 37 °C, 5% CO_2. Vero cells were maintained in DMEM containing 10% FBS, 1% Penicillin/Streptomycin and 1% L-Glutamine at 37 °C, 5% CO_2.

Primary hepatocyte coculture

Hepatic stellate cell line (CFSC-8B), used as a feeder cell layer, was plated at 10^6 cells per 25 cm^2 culture flasks in minimal essential medium (MEM, Invitrogen) supplemented with 10% fetal bovine serum (FBS), antibiotics (penicillin/streptomycin 100 IU/mL; Quality Biological), and 1% nonessential amino acids (Cellgro). After 2 h the MEM was replaced and 5×10^6 freshly isolated human hepatocytes suspension (Cambrex, Walkersville, MD) was seeded over the feeder cell line in a hepatocyte-defined medium (HDM, human hepatocyte growth medium). Following 3 h incubation, and monitoring cell attachment, the hepatocyte cocultures were grown in HDM comprised of: Dulbecco's modified Eagle medium (DMEM) with D-glucose 0.45%, L-glutamine 5 mM, without sodium pyruvate, and supplemented with albumin 0.2%, glucose 0.2%, galactose 0.2%, ornithine 0.01%, proline 0.003%, nicotinamide 0.061%, insulin-transferrin-sodium selinite (ITS, Sigma) 0.1%, $ZnCl_2$ 0.544 ug/mL, $ZnSO_4$ 0.75 ug/mL, $CuSO_4$ 0.2 ug/mL, $MnSO_4$ 0.025 ug/L, transforming growth factor-alpha (TGF-α) 20 ng/mL, and penicillin 100 units/mL, streptomycin 100 ug/mL, and dexamethasone 10^{-7} M. The HDM culture medium was replaced every 48 h. Primary hepatocyte cultures form spherical masses after 30 days in coculture. The hepatocyte cultures containing spherical masses were harvested with 0.05% trypsin in HDM (supplemented with 1% FBS) and reseeded at 5×10^4 cells/six-well plates and propagated in HDM (the plating efficiency was 90–95%). The monolayer cultures in six-well plates (which were used for most experiments) were reseeded at 10-day intervals. The "maintenance cultures" when allowed to grow for more than 4 weeks in HDM reform the spherical masses (from which monolayer culture of primary hepatocyte was derived as outlined). The "passage" numbers of post-attachment primary hepatocytes (PPH) cultures are recorded and refer to reseeding from the reformed primary hepatocyte containing spheroids in maintenance cultures. (Banaudha et al., 2010, 2011). For the MitoSOX staining experiment, a frozen stock of primary hepatocytes was thawed and seeded in collagen coated eight well chamber slides (BD Biocoat Collagen Type I cellware), at a density of 100,000 cells per well. Vero cells were also seeded on the same slides (50,000 cells per well) to serve as positive control for infection. Following an overnight incubation to allow attachment, one extra well of primary hepatocytes was gently washed once with media and subsequently a viable cell count was obtained for the well as described in the section below (Cell Viability Assays). Subsequently, the following treatment conditions were set up: (A) uninfected (control); (B) infection with recombinant MP-12 (rMP-12) at MOI 3; (C) infection with UV-inactivated recombinant MP-12 (rMP-12) at MOI 3; (D) infection with ΔNSs mutant derivative at MOI 3.The virus was removed after 1 h and replaced with media. MitoSOX staining to detect reactive oxygen species was performed as described below in the methods section (Reactive oxygen species detection).

Cell viability assays

Primary hepatocytes were seeded in collagen coated eight well chamber slides (BD Biocoat Collagen Type I cellware), at 100,000 cells per well, and cell viability was measured after 24 h, just prior to the start of infections. For viability measurement, the cells were trypsinized and washed with media. A volume of 10 μl of cell suspension was then mixed with 10 Trypan blue staining solution and 10 μl of this mix was used to count the number of live cells by a hemocytometer

Viral infections and protein extract preparation

HepG2 cells were seeded at a density of 1×10^6 cells per well in 6-well plates. The cells were infected with MP-12 for 1 h to allow for viral adsorption at 37 °C. The viral inoculum was removed and replaced with media. The cells were incubated for appropriate time frames at 37 °C, 5% CO_2. To prepare cell lysates, the media was removed and the cells were washed twice with PBS. Following the PBS wash, the cells were lysed with lysis buffer that consisted of a 1:1 mixture of T-PER reagent (Pierce, IL), 2X Tris-glycine SDS sample buffer (Novex, Invitrogen), 2.5% β-mercaptoethanol, and protease and phosphatase inhibitor cocktail (1X Halt cocktail, Pierce). The cell lysates were collected and boiled for 10 min and stored at −80 °C until analyzed.

Reactive oxygen species detection

To detect ROS in infected cells, 1×10^5 HepG2 cells were seeded per well in an eight-chamber slide. The slides were incubated at 37 °C, 5% CO_2 overnight and infected with MP-12, MP-12ΔNSs or MP-12ΔNSm as described earlier. At appropriate time points following infection, MitoSox reagent (Invitrogen, Cat#M36008) was added according to manufacturer's instructions (Narayanan et al., 2011). Cells were imaged using Nikon Eclipse TE2000-U. EZ-C1 software was used to perform statistical analysis to quantify fluorescence intensities.

Crude mitochondrial preparation

Cells were trypsinized and washed with cold PBS. The washed cells were resuspended in five times the pellet volume of cold isolation buffer that consisted of Mannitol (0.3 M), BSA (0.1%), EDTA (0.2 mM EDTA), HEPES (10 mM) and pH adjusted to 7.4 with KOH. The cell pellet was sheared by passing through a 22-gauge needle multiple times and the resultant lysate centrifuged at 1000 g for 10 min at 4 °C. The pellet was discarded and the supernatant spun at 14,000 g for 15 min at 4 °C. The supernatant was saved as the cytoplasmic fraction and the pellet saved as the mitochondrial fraction. The pellet was washed twice with cold isolation buffer, diluted in SDS containing buffer and electrophoresed.

Immunoprecipitation

HepG2 cells were infected with Flag-NSs-MP-12 virus (MOI: 5) and maintained at 37 °C for 24 h. Cells were pelleted and lysed in a buffer containing Tris–HCl (pH 7.5), NaCl (120 mM), EDTA (5 mM), NP-40 (0.5%), NaF (50 mM), Na3VO4 (0.2 mM), DTT (1 mM) and one tablet complete protease inhibitor cocktail per 50 ml. Lysis was performed under ice-cold conditions where the cell pellets were incubated with buffer on ice for 30 min and spun at 4 °C for 5 min at 14,000 rpm. Supernatant was transferred to a new tube and protein was quantitated with Bradford protein assay (BioRad, Hercules, CA, USA). Whole cell extract (~2 mg) was incubated overnight, rotating, at 4 °C with α-IgG, or α-Flag antibody. The next day, 30 μl of a 30% slurry of Protein A+G beads (Calbiochem, Rockland, MA) was added to the IPs and incubated for 2 h, rotating, at 4 °C. The IPs were spun briefly and beads were washed 1× with TNE150+0.1% NP-40, followed by a 1× wash with TNE50+0.1% NP-40. The beads were directly lysed with Urea (8M) after which the supernatant was processed for mass spectrometry.

Mass spectrometry

LC-MS/MS analysis was carried out as previously described (Narayanan et al., 2012). Briefly, samples were first lysed in 8M urea, after which, they were reduced using DTT and acetylated using iodoacetamide. The reduced and alkylated proteins were trypsin digested (Trypsin, Promega) for 4 h at 37 °C. The digested peptides were eluted using ZipTip purification (Millipore) and identification of the peptides was performed by LTQ-tandem MS/MS equipped with a reverse-phase liquid chromatography nanospray (ThermoFisher). After sample injection, the column was washed for 5 min at 200 nl/min with 0.1% formic acid; peptides were eluted using a 50-min linear gradient from 0 to 40% acetonitrile and an additional step of 80% acetonitrile (all in 0.1% formic acid) for 5 min. The LTQ-MS was operated in a data-dependent mode in which each full MS scan was followed by five MS-MS scans where the five most abundant molecular ions were dynamically selected and fragmented by collision-induced dissociation using normalized collision energy of 35%. Tandem mass spectra were matched against the National Center for Biotechnology Information mouse database by Sequest Bioworks software (ThermoFisher) using full tryptic cleavage constraints and static cysteine alkylation by iodoacetamide.

Immunofluorescence

HepG2 cells were seeded at 1×10^6 cells per well on coverslips in a 6-well plate. The cells were infected with MP-12 as described earlier. At appropriate time points, cells were fixed with 4% paraformaldehyde for 20 min. Cells were permeabilized with 0.5% Triton X-100 in PBS for 15 min. Slides were washed with PBS and blocked at room temperature for 10 min with 1% FBS. The slides were incubated with α-FLAG, α-Tomm20 (Abcam, Cat# ab78547), p65 (Cell Signaling, Cat# 4764S), p53 (Cell Signaling, Cat# 9282S) primary antibody for 1 h in the dark at 37 °C. The slides were washed three times with PBS and incubated with secondary antibodies for 1 h in the dark at 37 °C. Slides were washed three times with PBS and incubated with DAPI for 10 min in the dark at room temperature. Slides were washed once with PBS and mounted with Fluoromount G (SouthernBiotech, Cat#0100-01) and stored in the dark, at 4 °C overnight. The cells were imaged using Nikon Eclipse TE2000-U.

Column fractionation

The details of the column fractionation approach have been extensively described previously (Narayanan et al., 2012a, 2012b; Kehn-Hall et al., 2012). Briefly, HepG2 cells were seeded in T-150 flasks and incubated until confluent. A flask was infected with MP-12 virus (MOI: 10). Twenty-four hours post infection, the cells were harvested and pelleted by centrifugation (1200 rpm for 10 min at 4 °C). The cell pellets were lysed (50 mM Tris– HCl (pH 7.5), 120 mM NaCl, 5 mM ethylenediaminetetraacetic acid, 0.5% NP-40, 50 mM NaF, 0.2 mM Na_3VO_4, 1 mM DTT, and one complete protease cocktail tablet/50 mL) and 2 mg of protein was used for chromatography using a Superose 6 h 10/30 size-exclusion chromatography column and an AKTA purifier system (GE Healthcare, Piscataway, NJ, USA). A quarter inch gap was introduced to the top of the Superose 6 column to better separate small molecular weight complexes from fractions eluting off the far right side of the chromatogram. After sample injection (using 1 ml loop), running buffer was set at a flow rate of 0.3 ml/min and 0.5 ml fractions of the flow-through were collected at 4 °C for a total of approximately 50 fractions. The columns employed in this study were used for multiple runs prior to fractionation of the actual virus-infected or uninfected control extracts. This is a critical step to ensure reproducibility of fractionation profiles. Approximately 50 fractions were collected and fractions spanning a range of 1 mDa to 100 kDa were acetone precipitated using four volumes of ice-cold 100% acetone. Lysates were centrifuged at 4 °C f or 10 min at 12,000 rpm, supernatants were removed, and the pellets were allowed to dry for a few minutes at room temperature. The pellets were resuspended in Laemmli buffer and analyzed by immunoblotting for p65, p53 and β-actin.

Western blot analysis

Whole cell or fractionated lysates were separated on a 4–20% Tris-Glycine Gel and transferred to a polyvinyl difluoride (PVDF) membrane using the iBlot gel transfer system (Invitrogen). The membranes were blocked in 1% dry milk in PBS-T at room temperature. Primary antibodies to RVFV (ProSci, Cat# 4519), total p65 (Santa Cruz Biotechnology, Inc. Cat# sc7151), phospho-p65 (ser536) (Santacruz biotechnology, Inc., Cat# 33020), total p53 (Cell Signaling, Cat# 9282S), phospho-p53 (Ser15) (Cell Signaling, Cat# 9284S), Cytochrome C (Abcam, Cat# ab13575) and HRP conjugated actin (Abcam, Cat# ab49900) were used according to manufacturer's instructions and the blots were incubated overnight at 4 °C. The blots were washed three times with PBS-T and incubated with secondary HRP coupled goat anti-rabbit antibody (Cell Signaling, Cat# 7074). The blots were visualized by chemiluminescence using SuperSignal West Femto Maximum Sensitivity Substrate Kit (ThermoScientific) and a BIO-RAD Molecular Imager ChemiDoc XRS system (BIO-RAD). Signal intensities were calculated using Quantity One 4.6.5 software (BIO-RAD).

Quantitative RT-PCR

To determine expression of IL2, IL4, IL6 and IL8 following RVFV infection, 1×10^6 cells were seeded in a 6-well plate. Infections were carried out as described earlier and total RNA was isolated using the Qiagen RNeasy mini kit (Qiagen, Cat#74104) as per manufacturer's instructions. Isolated RNA was converted to cDNA and directly utilized to determine gene expression profiles of using primers to IL2, IL4, IL6 and IL8. The primers used for the PCRs are as follows:

IL2 fwd: 5′ AAC TCC TGT CTT GCA TTG CAC 3′
IL2 rev: 5′ GCT CCA GTT GTA GCT GTG TTT 3′
IL4 fwd: 5′ CCA ACT GCT TCC CCC TCT G 3′
IL4 rev: 5′ TCT GTT ACG GTC AAC TCG GTG 3′
IL6 fwd: 5′ ACT CAC CTC TTC AGA ACG AAT TG 3′
IL6 rev: 5′ GTC GAG GAT GTA CCG AAT TTG T 3′.

Details of the IL8 primers have been published (Mahieux et al., 2001). All reactions were carried out in triplicate, and gene expression levels were calculated relative to GAPDH levels or 18s RNA levels as endogenous controls. Relative expression was calculated as 2 (Ct gene under investigation − Ct GAPDH).

Rt-PCR

In order to determine IL8 expression, 1×10^6 HepG2 cells were seeded in a 6-well plate and infected with MP-12 as described earlier. Total RNA was isolated using the Qiagen RNeasy mini kit and cDNA was generated using Superscript Reverse Transcriptase cDNA kit (Invitrogen, Cat# 11917-010). The cDNA was utilized to perform RT-PCR reactions (35 cycles). The PCR products were resolved in 2% agarose gels and stained with ethidium bromide. The stained gels were visualized using the Bio Rad Molecular Imager ChemiDoc XRS system (Bio Rad) and band intensities were calculated using Quantity One 4.6.5 software (Bio Rad).

ELISA and hydrogel nanoparticles

Evaluation of secreted IL8 was performed using standard ELISA methods using the human IL8 ELISA kit from BD biosciences (BD OptEIA, Cat#550999) following manufacturer's instructions. The hydrogel nanoparticles used to concentrate IL8 from culture supernatants have been described in detail previously (Polyak et al., 2001a, 2001b; Tamburro et al., 2011). When hydrogel nanoparticles were utilized for sample concentration, 8 ml of culture supernatant was mixed with 1 ml of hydrogel nanoparticles (Cibacron blue bait and VSA shell) and incubated for 1 h at room temperature. The particles were then centrifuged at high speed (10,000 rpm for 15 min) and resuspended in 1 ml of water. Particle bound IL8 was eluted by washing particles with NaSCN (0.25M) and eluting using a 70% acetonitrile, 10% ammonium hydroxide buffer (Polyak et al., 2001b). Samples were dried using a Speed Vac (ThermoFisher) and resuspended in 100 ul of water. The samples were then analyzed by ELISA.

Inhibitor studies

HepG2 cells were seeded in 96-well plates at 5×10^4 cells/well 24 h prior to infection. For confocal experiments, cells were seeded in 8-chambered slides. Cells were pretreated with inhibitors Curcumin (Santacruz biotechnology, Inc., Cat# sc-200509) and Quercetin (Sigma, Cat# Q4951) for 2 h. The conditioned media (media containing inhibitor) was removed and viral infections were conducted for 1 h. The viral inoculum was removed and replaced with conditioned media. The cells were incubated for a further 24 h at 37 °C, 5% CO_2 and subsequently lysed for analysis.

Plaque assay

Quantification of infectious particles from viral supernatants was determined by plaque assay. Vero cells were seeded at a density of 5×10^5 cells per well in a 6-well plate. The next day, dilutions of viral supernatants were made in DMEM, and applied to wells in duplicate. Plates were incubated at 37 °C, 5% CO_2 for 1 h with occasional rocking. A 3 ml overlay comprising 2X E-MEM and 0.6% agarose (1:1) was added to each of the wells. Once solidified, the plates were incubated for an additional 72 h at 37 °C, 5% CO_2. Addition of a 10% Formaldehyde solution was applied to the surface of the agarose plugs for 1 h at room temperature. The plates were then rinsed with a gentle stream of diH_2O and the agarose plugs removed. A 1% crystal violet solution was added to each of the wells at room temperature with rocking for 30 min. The plates were rinsed with diH2O and visible plaques were counted to determine viral titers as PFU/mL.

Statistical analysis

Triplicate data points were averaged and mean was graphed unless otherwise indicated. Comparisons between groups was carried out using the unpaired Students *t*-test. *P* values were calculated by the unpaired Students *t*-test using Excel software. Statistical significance was set at $P < 0.05$ unless otherwise indicated.

Acknowledgments

The authors would like to thank Dr. Shinji Makino (UTMB) for the MP-12dNSs, MP-12ΔNSm, MP-12-Flag-NSs, and MP-12ΔNSs-GFP viruses. The authors thank members of the CAPMM laboratory at GMU for assistance with experiments involving the hydrogel nanoparticles. This work was supported by a United States Department of Energy grant DE-FC52-04NA25455 to FK and CB and USAMRIID contract funding W81XWH-11-P-0310 to RMH.

Appendix A. Supplementary material

Supplementary data associated with this article can be found in the online version at http://dx.doi.org/10.1016/j.virol.2013.11.023.

References

Abdalla, M.Y., Ahmad, I.M., Spitz, D.R., Schmidt, W.N., Britigan, B.E., 2005. Hepatitis C virus-core and non structural proteins lead to different effects on cellular antioxidant defenses. J. Med. Virol. 76, 489–497.
Abdalla, M.Y., Mathahs, M.M., Ahmad, I.M., 2012. Reduced heme oxygenase-1 expression in steatotic livers infected with hepatitis C virus. Eur. J. Intern. Med. 23, 649–655.
Aftab, N., Vieira, A., 2010. Antioxidant activities of curcumin and combinations of this curcuminoid with other phytochemicals. Phytother. Res. 24, 500–502.
Amraoui, F., Krida, G., Bouattour, A., Rhim, A., Daaboub, J., et al., 2012. Culex pipiens, an experimental efficient vector of West Nile and Rift Valley fever viruses in the Maghreb region. PLoS One 7, e36757.
Austin, D., Baer, A., Lundberg, L., Shafagati, N., Schoonmaker, A., et al., 2012. p53 Activation following Rift Valley fever virus infection contributes to cell death and viral production. PLoS One 7, e36327.
Baer, A., Austin, D., Narayanan, A., Popova, T., Kainulainen, M., et al., 2012. Induction of DNA damage signaling upon Rift Valley fever virus infection results in cell cycle arrest and increased viral replication. J. Biol. Chem. 287, 7399–7410.
Balasubramanian, A., Munshi, N., Koziel, M.J., Hu, Z., Liang, T.J., et al., 2005. Structural proteins of Hepatitis C virus induce interleukin 8 production and apoptosis in human endothelial cells. J. Gen. Virol. 86, 3291–3301.
Banaudha, K., Orenstein, J.M., Korolnek St, T., Laurent, G.C., Wakita, T., et al., 2010. Primary hepatocyte culture supports hepatitis C virus replication: a model for infection-associated hepatocarcinogenesis. Hepatology 51, 1922–1932.

Banaudha, K., Kaliszewski, M., Korolnek, T., Florea, L., Yeung, M.L., et al., 2011. MicroRNA silencing of tumor suppressor DLC-1 promotes efficient hepatitis C virus replication in primary human hepatocytes. Hepatology 53, 53–61.
Bantel, H., Schulze-Osthoff, K., 2003. Apoptosis in hepatitis C virus infection. Cell Death Differ. 10 (Suppl 1), S48–S58.
Beckman, J.S., Koppenol, W.H., 1996. Nitric oxide, superoxide, and peroxynitrite: the good, the bad, and ugly. Am. J. Physiol. 271, C1424–C1437.
Benferhat, R., Josse, T., Albaud, B., Gentien, D., Mansuroglu, Z., et al., 2012. Large-scale chromatin immunoprecipitation with promoter sequence microarray analysis of the interaction of the NSs protein of rift valley fever virus with regulatory DNA regions of the host genome. J. Virol. 86, 11333–11344.
Bird, B.H., Maartens, L.H., Campbell, S., Erasmus, B.J., Erickson, B.R., et al., 2011. Rift Valley fever virus vaccine lacking the NSs and NSm genes is safe, nonteratogenic, and confers protection from viremia, pyrexia, and abortion following challenge in adult and pregnant sheep. J. Virol. 85, 12901–12909.
Bouloy, M., Weber, F., 2010. Molecular biology of rift valley Fever virus. Open Virol. J. 4, 8–14.
Caplen, H., Peters, C.J., Bishop, D.H., 1985. Mutagen-directed attenuation of Rift Valley fever virus as a method for vaccine development. J. Gen. Virol. 66 (Pt 10), 2271–2277.
Chalaris, A., Rabe, B., Paliga, K., Lange, H., Laskay, T., et al., 2007. Apoptosis is a natural stimulus of IL6R shedding and contributes to the proinflammatory trans-signaling function of neutrophils. Blood 110, 1748–1755.
Chen, L., Fischle, W., Verdin, E., Greene, W.C., 2001. Duration of nuclear NF-kappaB action regulated by reversible acetylation. Science 293, 1653–1657.
Chen, L.F., Mu, Y., Greene, W.C., 2002. Acetylation of RelA at discrete sites regulates distinct nuclear functions of NF-kappaB. EMBO J. 21, 6539–6548.
de Boer, S.M., Kortekaas, J., Antonis, A.F., Kant, J., van Oploo, J.L., et al., 2010. Rift Valley fever virus subunit vaccines confer complete protection against a lethal virus challenge. Vaccine 28, 2330–2339.
Ding, X., Xu, F., Chen, H., Tesh, R.B., Xiao, S.Y., 2005. Apoptosis of hepatocytes caused by Punta Toro virus (Bunyaviridae: Phlebovirus) and its implication for Phlebovirus pathogenesis. Am. J. Pathol. 167, 1043–1049.
Dodd, K.A., Bird, B.H., Metcalfe, M.G., Nichol, S.T., Albarino, C.G., 2012. Single-dose immunization with virus replicon particles confers rapid robust protection against Rift Valley fever virus challenge. J. Virol. 86, 4204–4212.
Duran, A., Rodriguez, A., Martin, P., Serrano, M., Flores, J.M., et al., 2004. Crosstalk between PKCzeta and the IL4/Stat6 pathway during T-cell-mediated hepatitis. EMBO J. 23, 4595–4605.
Duygu, F., Karsen, H., Aksoy, N., Taskin, A., 2012. Relationship of oxidative stress in hepatitis B infection activity with HBV DNA and fibrosis. Ann. Lab. Med. 32, 113–118.
Farias, M.S., Budni, P., Ribeiro, C.M., Parisotto, E.B., Santos, C.E., et al., 2012. Antioxidant supplementation attenuates oxidative stress in chronic hepatitis C patients. Gastroenterol. Hepatol. 35, 386–394.
Filone, C.M., Hanna, S.L., Caino, M.C., Bambina, S., Doms, R.W., et al., 2010. Rift valley fever virus infection of human cells and insect hosts is promoted by protein kinase C epsilon. PLoS One 5, e15483.
Fredolini, C., Meani, F., Reeder, K.A., Rucker, S., Patanarut, A., et al., 2008. Concentration and preservation of very low abundance biomarkers in urine, such as human growth hormone (hGH), by cibacron blue F3G-A loaded hydrogel particles. Nano Res. 1, 502–518.
Furia, B., Deng, L., Wu, K., Baylor, S., Kehn, K., et al., 2002. Enhancement of nuclear factor-kappa B acetylation by coactivator p300 and HIV-1 Tat proteins. J. Biol. Chem. 277, 4973–4980.
Gauliard, N., Billecocq, A., Flick, R., Bouloy, M., 2006. Rift Valley fever virus noncoding regions of L, M and S segments regulate RNA synthesis. Virology 351, 170–179.
Gong, G., Waris, G., Tanveer, R., Siddiqui, A., 2001. Human hepatitis C virus NS5A protein alters intracellular calcium levels, induces oxidative stress, and activates STAT-3 and NF-kappa B. Proc. Natl. Acad. Sci. U. S. A. 98, 9599–9604.
Gwinn, M.R., Vallyathan, V., 2006. Respiratory burst: role in signal transduction in alveolar macrophages. J. Toxicol. Environ. Health B Crit. Rev. 9, 27–39.
Habjan, M., Pichlmair, A., Elliott, R.M., Overby, A.K., Glatter, T., et al., 2009. NSs protein of rift valley fever virus induces the specific degradation of the double-stranded RNA-dependent protein kinase. J. Virol. 83, 4365–4375.
Ikegami, T., 2012. Molecular biology and genetic diversity of Rift Valley fever virus. Antiviral. Res. 95, 293–310.
Ikegami, T., Makino, S., 2009. Rift valley fever vaccines. Vaccine 27 (Suppl 4), D69–D72.
Ikegami, T., Makino, S., 2011. The pathogenesis of Rift Valley fever. Viruses 3, 493–519.
Ikegami, T., Won, S., Peters, C.J., Makino, S., 2005a. Rift Valley fever virus NSs mRNA is transcribed from an incoming anti-viral-sense S RNA segment. J. Virol. 79, 12106–12111.
Ikegami, T., Peters, C.J., Makino, S., 2005b. Rift valley fever virus nonstructural protein NSs promotes viral RNA replication and transcription in a minigenome system. J. Virol. 79, 5606–5615.
Ikegami, T., Won, S., Peters, C.J., Makino, S., 2006. Rescue of infectious rift valley fever virus entirely from cDNA, analysis of virus lacking the NSs gene, and expression of a foreign gene. J. Virol. 80, 2933–2940.
Ikegami, T., Narayanan, K., Won, S., Kamitani, W., Peters, C.J., et al., 2009a. Rift Valley fever virus NSs protein promotes post-transcriptional downregulation of protein kinase PKR and inhibits eIF2alpha phosphorylation. PLoS Pathog. 5, e1000287.
Ikegami, T., Narayanan, K., Won, S., Kamitani, W., Peters, C.J., et al., 2009b. Dual functions of Rift Valley fever virus NSs protein: inhibition of host mRNA transcription and post-transcriptional downregulation of protein kinase PKR. Ann. N. Y. Acad. Sci. 1171 (Suppl 1), E75–E85.
Imai, Y., Kuba, K., Neely, G.G., Yaghubian-Malhami, R., Perkmann, T., et al., 2008. Identification of oxidative stress and Toll-like receptor 4 signaling as a key pathway of acute lung injury. Cell 133, 235–249.
Ivanov, A.V., Smirnova, O.A., Ivanova, O.N., Masalova, O.V., Kochetkov, S.N., et al., 2011. Hepatitis C virus proteins activate NRF2/ARE pathway by distinct ROS-dependent and independent mechanisms in HUH7 cells. PLoS One 6, e24957.
Jackson, J.K., Higo, T., Hunter, W.L., Burt, H.M., 2006. The antioxidants curcumin and quercetin inhibit inflammatory processes associated with arthritis. Inflamm. Res. 55, 168–175.
Jaeschke, H., 2011. Reactive oxygen and mechanisms of inflammatory liver injury: Present concepts. J. Gastroenterol. Hepatol. 26 (Suppl 1), 173–179.
Jain, A.K., Allton, K., Iacovino, M., Mahen, E., Milczarek, R.J., et al., 2012. p53 regulates cell cycle and microRNAs to promote differentiation of human embryonic stem cells. PLoS Biol. 10, e1001268.
Jansen van Vuren, P., Tiemessen, C.T., Paweska, J.T., 2011. Anti-nucleocapsid protein immune responses counteract pathogenic effects of Rift Valley fever virus infection in mice. PLoS One 6, e25027.
Kalveram, B., Lihoradova, O., Ikegami, T., 2011. NSs protein of rift valley fever virus promotes posttranslational downregulation of the TFIIH subunit p62. J. Virol. 85, 6234–6243.
Kalveram, B., Lihoradova, O., Indran, S.V., Ikegami, T., 2011. Using reverse genetics to manipulate the NSs gene of the Rift Valley fever virus MP-12 strain to improve vaccine safety and efficacy. J. Vis. Exp., e3400.
Kalveram, B., Lihoradova, O., Indran, S.V., Lokugamage, N., Head, J.A., Ikegami, T., 2013. Rift Valley fever virus NSs inhibits host transcription independently of the degradation of dsRNA-dependent protein kinase PKR. Virology 435 (2), 415–424.
Kehn-Hall, K., Narayanan, A., Lundberg, L., Sampey, G., Pinkham, C., et al., 2012. Modulation of GSK-3beta activity in Venezuelan equine encephalitis virus infection. PLoS One 7, e34761.
Kim, W.J., Rivera, M.N., Coffman, E.J., Haber, D.A., 2012. The WTX tumor suppressor enhances p53 acetylation by CBP/p300. Mol. Cell 45, 587–597.
Komita, H., Homma, S., Saotome, H., Zeniya, M., Ohno, T., et al., 2006. Interferon-gamma produced by interleukin-12-activated tumor infiltrating CD8+T cells directly induces apoptosis of mouse hepatocellular carcinoma. J. Hepatol. 45, 662–672.
Korenaga, M., Wang, T., Li, Y., Showalter, L.A., Chan, T., et al., 2005. Hepatitis C virus core protein inhibits mitochondrial electron transport and increases reactive oxygen species (ROS) production. J. Biol. Chem. 280, 37481–37488.
Kortekaas, J., Antonis, A.F., Kant, J., Vloet, R.P., Vogel, A., et al., 2012. Efficacy of three candidate Rift Valley fever vaccines in sheep. Vaccine 30, 3423–3429.
Lacour, S., Gautier, J.C., Pallardy, M., Roberts, R., 2005. Cytokines as potential biomarkers of liver toxicity. Cancer Biomark 1, 29–39.
Le May, N., Mansuroglu, Z., Leger, P., Josse, T., Blot, G., et al., 2008. A SAP30 complex inhibits IFN-beta expression in Rift Valley fever virus infected cells. PLoS Pathog. 4, e13.
Lin, W., Wu, G., Li, S., Weinberg, E.M., Kumthip, K., et al., 2011. HIV and HCV cooperatively promote hepatic fibrogenesis via induction of reactive oxygen species and NFkappaB. J. Biol. Chem. 286, 2665–2674.
Longo, C., Patanarut, A., George, T., Bishop, B., Zhou, W., et al., 2009. Core-shell hydrogel particles harvest, concentrate and preserve labile low abundance biomarkers. PLoS One 4, e4763.
Mahieux, R., Lambert, P.F., Agbottah, E., Halanski, M.A., Deng, L., et al., 2001. Cell cycle regulation of human interleukin-8 gene expression by the human immunodeficiency virus type 1 Tat protein. J. Virol. 75, 1736–1743.
Mandell, R.B., Koukuntla, R., Mogler, L.J., Carzoli, A.K., Freiberg, A.N., et al., 2010. A replication-incompetent Rift Valley fever vaccine: chimeric virus-like particles protect mice and rats against lethal challenge. Virology 397, 187–198.
Mansuroglu, Z., Josse, T., Gilleron, J., Billecocq, A., Leger, P., et al., 2010. Nonstructural NSs protein of rift valley fever virus interacts with pericentromeric DNA sequences of the host cell, inducing chromosome cohesion and segregation defects. J. Virol. 84, 928–939.
Morrill, J.C., Peters, C.J., 2011. Protection of MP-12-vaccinated rhesus macaques against parenteral and aerosol challenge with virulent rift valley fever virus. J. Infect. Dis. 204, 229–236.
Moser, T.S., Schieffer, D., Cherry, S., 2012. AMP-activated kinase restricts Rift Valley fever virus infection by inhibiting fatty acid synthesis. PLoS Pathog. 8, e1002661.
Narayanan, A., Popova, T., Turell, M., Kidd, J., Chertow, J., et al., 2011. Alteration in superoxide dismutase 1 causes oxidative stress and p38 MAPK activation following RVFV infection. PLoS One 6, e20354.
Narayanan, A., Kehn-Hall, K., Senina, S., Lundberg, L., Van Duyne, R., et al., 2012a. Curcumin inhibits Rift Valley fever virus replication in human cells. J. Biol. Chem. 287, 33198–33214.
Narayanan, A., Sampey, G., Van Duyne, R., Guendel, I., Kehn-Hall, K., et al., 2012b. Use of ATP analogs to inhibit HIV-1 transcription. Virology 432, 219–231.
Piccoli, C., Scrima, R., Quarato, G., D'Aprile, A., Ripoli, M., et al., 2007. Hepatitis C virus protein expression causes calcium-mediated mitochondrial bioenergetic dysfunction and nitro-oxidative stress. Hepatology 46, 58–65.
Pichlmair, A., Habjan, M., Unger, H., Weber, F., 2010. Virus-like particles expressing the nucleocapsid gene as an efficient vaccine against Rift Valley fever virus. Vector Borne Zoonotic. Dis. 10, 701–703.
Polyak, S.J., Khabar, K.S., Paschal, D.M., Ezelle, H.J., Duverlie, G., et al., 2001a. Hepatitis C virus nonstructural 5A protein induces interleukin-8, leading to partial inhibition of the interferon-induced antiviral response. J. Virol. 75, 6095–6106.

Polyak, S.J., Khabar, K.S., Rezeiq, M., Gretch, D.R., 2001b. Elevated levels of interleukin-8 in serum are associated with hepatitis C virus infection and resistance to interferon therapy. J. Virol. 75, 6209–6211.
Popova, T.G., Turell, M.J., Espina, V., Kehn-Hall, K., Kidd, J., et al., 2010. Reverse-phase phosphoproteome analysis of signaling pathways induced by Rift valley fever virus in human small airway epithelial cells. PLoS One 5, e13805.
Ramakrishnan, R., Liu, H., Donahue, H., Malovannaya, A., Qin, J., et al., 2012. Identification of novel CDK9 and Cyclin T1-associated protein complexes (CCAPs) whose siRNA depletion enhances HIV-1 Tat function. Retrovirology 9, 90.
Reed, C., Steele, K.E., Honko, A., Shamblin, J., Hensley, L.E., et al., 2012. Ultrastructural study of Rift Valley fever virus in the mouse model. Virology 431, 58–70.
Rodrigues, R., Paranhos-Baccala, G., Vernet, G., Peyrefitte, C.N., 2012. Crimean-Congo hemorrhagic fever virus-infected hepatocytes induce ER-stress and apoptosis crosstalk. PLoS One 7, e29712.
Seufi, A.M., Galal, F.H., 2010. Role of Culex and Anopheles mosquito species as potential vectors of rift valley fever virus in Sudan outbreak, 2007. BMC Infect. Dis. 10, 65.
Sharma, R., Bagavant, H., Jarjour, W.N., Sung, S.S., Ju, S.T., 2005. The role of Fas in the immune system biology of IL-2R alpha knockout mice: interplay among regulatory T cells, inflammation, hemopoiesis, and apoptosis. J. Immunol. 175, 1965–1973.
Smith, D.R., Steele, K.E., Shamblin, J., Honko, A., Johnson, J., et al., 2010. The pathogenesis of Rift Valley fever virus in the mouse model. Virology 407, 256–267.
Smith, D.R., Bird, B.H., Lewis, B., Johnston, S.C., McCarthy, S., et al., 2012. Development of a novel nonhuman primate model for Rift Valley fever. J. Virol. 86, 2109–2120.
Tamburro, D., Fredolini, C., Espina, V., Douglas, T.A., Ranganathan, A., et al., 2011. Multifunctional core-shell nanoparticles: discovery of previously invisible biomarkers. J. Am. Chem. Soc. 133, 19178–19188.
Tawadrous, G.A., Aziz, A.A., Amin, D.G., Eldemery, A., Mostafa, M.A., 2012. RANTES, TNF-alpha, oxidative stress, and hematological abnormalities in hepatitis C virus infection. J. Investig. Med. 60, 878–882.
Terasaki, K., Murakami, S., Lokugamage, K.G., Makino, S., 2011. Mechanism of tripartite RNA genome packaging in Rift Valley fever virus. Proc. Natl. Acad. Sci. U. S. A. 108, 804–809.
Terasaki, K., Won, S., Makino, S., 2013. The C-terminal region of Rift Valley fever virus NSm protein targets the protein to the mitochondrial outer membrane and exerts antiapoptotic function. J. Virol. 87, 676–682.
Tonino, S.H., van Laar, J., van Oers, M.H., Wang, J.Y., Eldering, E., et al., 2011. ROS-mediated upregulation of Noxa overcomes chemoresistance in chronic lymphocytic leukemia. Oncogene 30, 701–713.
Turell, M.J., Linthicum, K.J., Patrican, L.A., Davies, F.G., Kairo, A., et al., 2008. Vector competence of selected African mosquito (Diptera: Culicidae) species for Rift Valley fever virus. J. Med. Entomol. 45, 102–108.
Turell, M.J., Wilson, W.C., Bennett, K.E., 2010b. Potential for North American mosquitoes (Diptera: Culicidae) to transmit rift valley fever virus. J. Med. Entomol. 47, 884–889.
Turell, M.J., Dohm, D.J., Geden, C.J., Hogsette, J.A., Linthicum, K.J., 2010a. Potential for stable flies and house flies (Diptera: Muscidae) to transmit Rift Valley fever virus. J. Am. Mosq. Control Assoc. 26, 445–448.
Ushio-Fukai, M., 2009. Compartmentalization of redox signaling through NADPH oxidase-derived ROS. Antioxid. Redox Signal 11, 1289–1299.
Vialat, P., Muller, R., Vu, T.H., Prehaud, C., Bouloy, M., 1997. Mapping of the mutations present in the genome of the Rift Valley fever virus attenuated MP12 strain and their putative role in attenuation. Virus Res. 52, 43–50.
Waris, G., Huh, K.W., Siddiqui, A., 2001. Mitochondrially associated hepatitis B virus X protein constitutively activates transcription factors STAT-3 and NF-kappa B via oxidative stress. Mol. Cell Biol. 21, 7721–7730.
Weaver, S.C., Reisen, W.K., 2010. Present and future arboviral threats. Antiviral. Res. 85, 328–345.
Won, S., Ikegami, T., Peters, C.J., Makino, S., 2007. NSm protein of Rift Valley fever virus suppresses virus-induced apoptosis. J. Virol. 81, 13335–13345.
Yang, T.C., Lai, C.C., Shiu, S.L., Chuang, P.H., Tzou, B.C., et al., 2010. Japanese encephalitis virus down-regulates thioredoxin and induces ROS-mediated ASK1-ERK/p38 MAPK activation in human promonocyte cells. Microbes. Infect. 12, 643–651.
Yee, J., White, R.E., Anderton, E., Allday, M.J., 2011. Latent Epstein-Barr virus can inhibit apoptosis in B cells by blocking the induction of NOXA expression. PLoS One 6, e28506.
Zhang, M., Swarts, S.G., Yin, L., Liu, C., Tian, Y., et al., 2011. Antioxidant properties of quercetin. Adv. Exp. Med. Biol. 701, 283–289.